JCTC Journal of Chemical Theory and Computation

Article

pubs.acs.org/JCTC

Coarse-Graining of TIP4P/2005, TIP4P-Ew, SPC/E, and TIP3P to Monatomic Anisotropic Water Models Using Relative Entropy Minimization

Jibao Lu,[†,‡] Yuqing Qiu,[†] Riccardo Baron,*[,‡] and Valeria Molinero*[,†]

[†]Department of Chemistry, The University of Utah, Salt Lake City, Utah 84112-0850, United States

[‡]Department of Medicinal Chemistry, The University of Utah, Salt Lake City, Utah 84112-5820, United States

ABSTRACT: Coarse-grained models are becoming a competitive alternative for modeling processes that occur over time and length scales beyond the reach of fully atomistic molecular simulations. Ideally, coarse-grained models should not only achieve high computational efficiency but also provide accurate predictions and fundamental insight into the role of molecular interactions, the characteristic behavior, and properties of the system they model. In this work we derive a series of monatomic coarse-grained water models mX^{REM} from the most popular atomistic water models X = TIP3P, SPC/E, TIP4P-Ew, and TIP4P/2005, using the relative entropy minimization (REM) method. Each coarse-grained water molecule is represented by a single particle that interacts through short-ranged anisotropic interactions that encourage the formation of "hydrogen-bonded" structures. We systematically investigate the features of the coarse-grained models in reproducing over 20 structural, dynamic, and thermodynamic properties of the reference atomistic water models—including the existence and locus of the characteristic density anomaly. The mX^{REM} coarse-grained models reproduce quite faithfully the radial and angular distribution function of water, produce a temperature of maximum density (TMD), and stabilize the ice I crystal. Moreover, the ratio between the TMD and the melting temperature of the crystal in the mX^{REM} models and liquid−ice equilibrium properties show reasonable agreement with the results of the corresponding atomistic models. The mX^{REM} models, however, severely underestimate the cohesive energy of the condensed water phases. We investigate which specific limitations of the coarse-grained models arise from the REM methodology, from the monatomic nature of the models, and from the Stillinger−Weber interaction potential form. Our analysis indicates that a small compromise in the accuracy of structural properties can result in a significant increase of the overall accuracy and representability of the coarse-grained water models. We evaluate the accuracy of the atomistic and the monatomic anisotropic coarse-grained water models, including the mW water model, in reproducing experimental water properties. We find that mW and mTIP4P/2005^{REM} score closer to experiment than widely used atomistic water models. We conclude that monatomic models of water with short-range, anisotropic "hydrogen-bonding" three-body interactions can be competitive in accuracy with fully atomistic models for the study of a wide range of properties and phenomena at less than 1/100th of the computational cost.

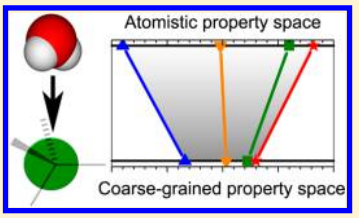

I. INTRODUCTION

Although water is a small and relatively simple molecule, reproducing its properties with molecular simulations is an enduring challenge.[1,2] Over a hundred molecular water models have been proposed since Bernal and Fowler's pioneering one in 1933.[3] These models represent water and its interactions according to various paradigms or approximations. Classical fully atomistic rigid nonpolarizable models that interact through electrostatic interactions and Lennard-Jones potentials constitute the most popular paradigm for modeling water. Vega and Abascal have provided an exhaustive appraisal of the capabilities and limitations of this class.[1] A central conclusion of their analysis is that an increase in the number of interaction sites does not necessarily result in an increase in overall accuracy.

Motivated by the quest of simulating larger spatiotemporal scales to study new phenomena, tremendous efforts are invested into developing computationally faster coarse-grained (CG) models that describe water at lower resolution by grouping atoms or molecules into few effective interaction sites.[4,5] Ideally, well-designed CG models should not only achieve high computational efficiency but also provide quantitatively accurate predictions and fundamental insight into the role of molecular interactions on the properties of water.

Coarse-grained models are defined by their resolution (e.g., one coarse-grained bead per water molecule), mapping (e.g., the bead position is the one of the oxygen atom), form of the interaction potential between particles (e.g., two-body spline functions), and method of parametrization. High-resolution coarse-grained water models represent each molecule as a single particle. These monatomic water models can be classified according to their interactions in two groups: those in which the interactions between molecules are isotropic,[6−10] and those that introduce anisotropic terms in the potential to represent the directionality of hydrogen-bonding interactions between water molecules.[11−16]

Received: June 5, 2014
Published: July 16, 2014

   dx.doi.org/10.1021/ct500487h | J. Chem. Theory Comput. 2014, 10, 4104−4120

Once the resolution, mapping scheme, and type of interactions of the CG representation is selected, the essential work to develop a CG model consists of deriving the appropriate interactions between the CG sites, which should capture the effects of the interactions vanished upon coarse-graining. In general, there are two main coarse-graining paradigms, namely, "top-down" and "bottom-up" approaches, to parametrize the potentials governing the site−site interactions.[17]

The top-down approach often employs interaction potentials with simple functional forms to describe the site−site interactions. It constructs the CG models by matching experimental observables, usually thermodynamic or structural properties, for a particular system. This approach could guarantee that the properties selected for the parametrization are all fully reproduced and transferable to different systems. However, in practice, representability issues can prevent combinations of these properties from being reproduced simultaneously.[7,18] Despite considerable progress in this direction,[19−21] matching the large-scale emergent phenomena may not necessarily result in accurate potentials for modeling water and complex molecules.[1,22,23]

Bottom-up approaches, on the other hand, parametrize the CG model on the basis of a more detailed model (typically an atomistic model), usually relying on a well-defined statistical mechanics framework.[24,25] The many-body potential of mean force (PMF)[26] is a central quantity in many bottom-up approaches to coarse-graining.[17,27−29] In the hypothetical limit that the many-body PMF of the more detailed model is explicitly determined in the CG model, the CG model will exactly reproduce, at the resolution of the CG mapping, all structural properties of the reference model. However, approximations to the many-body PMF must be made in practice because the explicit many-body PMF is too difficult to calculate for most systems,[30] and too complex, if it could be determined, for subsequent computations.[17]

To parametrize the CG potentials that optimally approximate the many-body PMF, a wide range of methodologies has been developed, such as Boltzmann inversion,[31,32] iterative Boltzmann inversion,[33] and inverse Monte Carlo[34,35] methods, which are based on reproducing target correlation functions determined by the atomistic level (AL) model and CG mapping, and the relative entropy minimization (REM)[36−38] method and the multiscale coarse-graining (MS-CG)[9,39] force matching methods, which are based on minimizing an appropriate functional to determine an approximate CG potential. A convenient aspect of bottom-up approaches is that they can in principle parametrize functions with a large number of independent variables, which enables the CG models to use flexible function forms (such as splines) to more accurately approximate the many-body PMF. Particularly, the REM and MS-CG approaches provide flexibility for numerically optimizing the CG potential because these approaches determine the CG interactions by minimizing a functional that is independent of the form of the CG potential,[17] which makes the parametrization of models with two- and three-body contributions practically feasible.[13,15]

Monatomic water models with isotropic pair interactions were developed by bottom-up approaches using MS-CG,[9] Boltzmann inversion,[7,40] and REM[10] with rigid nonpolarizable atomistic water models as reference systems. Isotropic water models derived to reproduce the radial distribution function of the AL water, however, do not reproduce the AL angular distribution function, underestimate the internal energy of the liquid by about 50%, and do not produce the more characteristic anomaly of liquid water: the existence of a density maximum.[7,8,10] It is possible, however, to recover the anomalous behavior of water with isotropic water models when a different effective pair interaction is derived for each state point.[10] To our knowledge, none of the monatomic isotropic water models stabilize a tetrahedrally coordinated crystal phase. This lack of transferability across thermodynamic state points and phases of water constitutes a significant limitation of isotropic monatomic water models.

Anisotropic interactions in monatomic water models have been introduced using three-body potentials that favor tetrahedral angles between triplets of molecules. The monatomic water model mW of Molinero and Moore is representative of this modeling paradigm.[11] Interactions in the mW model are represented by a sum of two-body and three-body terms with the functional form of the Stillinger−Weber (SW) potential,[41] parametrized top-down to reproduce the experimental melting temperature of hexagonal ice and the density and enthalpy of vaporization of liquid water at 298 K and 1 atm.[11] The three-body SW potential is anisotropic; i.e., it depends on the angles formed by water triplets that are within the cutoff distance that determines the extent of the "hydrogen-bonding" interactions in the model. We call the monatomic water models based on anisotropic potentials "anisotropic water models", although it should be noted that the coarse-grained particles themselves have no orientational degrees of freedom. The mW model produces the characteristic anomalies of liquid water and outperforms the most popular atomistic models of water in several key properties.[11] This indicates that the SW potential form has the flexibility to reproduce several *experimental* properties of water with good accuracy. Larini et al. have used the MS-CG force-matching approach to develop a bottom-up monatomic water model derived based on SPC/E water.[13,14] This coarse-grained model, which we term mSPC/E$^{MS\text{-}CG}$, uses the Stillinger−Weber cosine quadratic three-body term,[41] as in mW water, combined with two-body interactions based on splines.[13,14] The mSPC/E$^{MS\text{-}CG}$ model reproduces very well the radial distribution function of the AL model but severely underestimates the internal energy of liquid water, a shortcoming shared with the isotropic water models but not with mW. This poses the question of whether these representability issues arise from insufficient flexibility in the coarse-grained potential to mimic SPC/E or from some aspect of the parametrization method.

In this work, we use the bottom-up REM method[36−38] to develop a set of single-particle CG water models that interact through the anisotropic Stillinger−Weber potential.[41] We select a set of four popular rigid nonpolarizable models, X = TIP3P,[42] SPC/E,[43] TIP4P-Ew,[44] and TIP4P/2005,[45] as the reference models for the parametrization of the corresponding mX^{REM} monatomic CG water models. We use REM because its implementation for the two- and three-body functions of the SW potential is straightforward. We parametrize coarse-grained water models for three main reasons. First, water presents significant challenges for coarse-graining. Although a water molecule is small and relatively simple, its properties, phase behavior, and anomalies are notoriously difficult to reproduce. Second, over 80% of the computing time of explicit solvent simulations is spent on calculating interactions involving water, further motivating the need for efficient and accurate coarse-grained models. Third, the property spaces of some atomistic

water models are very close to each other, such as those of TIP4P-Ew[44] and TIP4P/2005,[45] which enables us to evaluate the ability of the REM method to discriminate among similar models and to analyze the effect of coarse-graining on the property space of the water models. We implement Vega and Abascal's test of water models[1] to score the ability of the mX^{REM} and mW models to reproduce thermodynamic, dynamic, and structural properties of their reference atomistic models and experiment, and to assess the representability of the coarse-grained water models.

II. METHODS

A. Models. In this work we employ the SW potential originally developed for silicon[41] and more recently used for the mW water model[11] as the CG site−site interaction potential in the set of one-bead CG mX^{REM} water models. Each water molecule is represented by a single particle that interacts through a sum of two-body ϕ_2 and three-body ϕ_3 interactions:

$$U = \sum_i \sum_{j>i} \phi_2(r_{ij}) + \sum_i \sum_{j\neq i} \sum_{k>j} \phi_3(r_{ij}, r_{ik}, \theta_{ijk}) \tag{1}$$

$$\phi_2 = A\epsilon\left[B\left(\frac{\sigma}{r_{ij}}\right)^p - 1\right]\exp\left(\frac{\sigma}{r_{ij} - a_2\sigma}\right) \tag{2}$$

$$\phi_3(r_{ij}, r_{ik}, \theta_{ijk}) = \lambda\epsilon[\cos\theta_{ijk} - \cos\theta_0]^2 \exp\left(\frac{\gamma\sigma}{r_{ij} - a_3\sigma}\right) \exp\left(\frac{\gamma\sigma}{r_{ik} - a_3\sigma}\right) \tag{3}$$

where $a_2\sigma$ and $a_3\sigma$ control the cutoffs of the two-body and three-body interactions, respectively, which ensures that the two- and three-body terms in the potential and forces go to zero at a distance $a_2\sigma$ and $a_3\sigma$, respectively. Note that in order to give more flexibility to the water potential, we have modified the original SW potential by splitting the cutoff-controlling parameter a into two separate parameters, a_2 and a_3, thus making the parameters in the two-body and three-body terms fully independent of each other. The simultaneous optimization of A and λ is not independent from ϵ, so we choose to keep A = 7.049556277 as in the original SW potential.[41] We also keep parameter p fixed to the original SW model value of 4 (we later test the dependence of the force field on p by changing it to p = 9 to allow for a steeper two-body repulsion). The remaining eight independent parameters of eq 2 and 3 (ϵ, σ, a_2, a_3, γ, B, λ, and cos θ_0) are simultaneously optimized during the REM process.

B. Relative Entropy Minimization Approach. The REM approach proposed by Shell and co-workers[36−38] is a variational method for optimizing the CG models based upon the information theoretic relative entropy, S_{rel}, which measures the information loss upon coarse-graining and is given by

$$S_{rel} = \sum_\nu p_{AL}(\nu) \ln\left[\frac{p_{AL}(\nu)}{p_{CG}(M(\nu))}\right] + S_{map} \tag{4}$$

where $p_X(\nu)$ is the equilibrium ensemble probability of a particular configuration ν, using model X. M is a mapping operator for turning an AL configuration ν to a CG configuration $M(\nu)$. The summation is over the set of all AL configurations ν. S_{map} is the so-called mapping entropy that stems from the average degeneracy of AL configurations mapping to the same CG one,[36,37] and it is independent of the CG force field. The canonical expression for the relative entropy is obtained by substitution of the Boltzmann configurational probabilities in eq 4,

$$S_{rel} = \beta\langle U_{CG} - U_{AL}\rangle_{AL} - \beta(A_{CG} - A_{AL}) + S_{map} \tag{5}$$

Here, $\beta = 1/\kappa_B T$, U is the total potential energy, $A = -\kappa_B T \ln Z$ is the configurational Helmholtz free energy, where Z is the canonical partition function, and the ensemble average $\langle U_{CG} - U_{AL}\rangle_{AL}$ is performed in the AL ensemble.

The CG model's force field is optimized by minimizing S_{rel} between a CG model and a reference AL model. To minimize the relative entropy, instead of directly evaluating S_{rel} (which is difficult due to its dependence on the Helmholtz free energies of the AL and CG systems), it is more effective to compute the derivatives of the relative entropy in parameter space,[38] which can be minimized by steepest descent or other minimization procedures. The first derivatives are given by

$$\frac{\partial S_{rel}}{\partial q} = \beta\left\langle \frac{\partial U_{CG}}{\partial q}\right\rangle_{AL} - \beta\left\langle \frac{\partial U_{CG}}{\partial q}\right\rangle_{CG} \tag{6}$$

where q is a vector composed of the set of all CG potential parameters q_i. The second derivative (Hessian matrix) is given by

$$\mathcal{H}_{ij} = \beta\left\langle \frac{\partial^2 U_{CG}}{\partial q_i\,\partial q_j}\right\rangle_{AL} - \beta\left\langle \frac{\partial^2 U_{CG}}{\partial q_i\,\partial q_j}\right\rangle_{CG} + \beta^2\left\langle \frac{\partial U_{CG}}{\partial q_i}\frac{\partial U_{CG}}{\partial q_j}\right\rangle_{CG} - \beta^2\left\langle \frac{\partial U_{CG}}{\partial q_i}\right\rangle_{CG}\left\langle \frac{\partial U_{CG}}{\partial q_j}\right\rangle_{CG} \tag{7}$$

C. Implementation of the REM Approach and Validation of the Code. In this work, we implement the REM method into the LAMMPS software.[46] The relative entropy with respect to the model parameters (q) is minimized based on two standard numerical techniques, steepest descent and Newton−Raphson minimization algorithms. These approaches use the derivatives, which are calculated analytically, to step iteratively through parameter space toward the relative entropy minimum, where the first derivative, $\partial S_{rel}/\partial q$, equals zero.

To validate our implementation of the REM in LAMMPS, we perform a series of test runs in which we recover the parameters of the mW water model from different initial parameter spaces. For all of the sets, the parameters are recovered with high numerical precision ($\lesssim$0.5% error for B, which has the biggest fluctuation, and $\lesssim$0.2% error for the other parameters), giving high consistency in parameters and properties with the original mW model. A further verification for $TIP4P/2005^{REM}$ also results in essentially identical final CG parameters when starting from arbitrary different values.

D. Simulation Details. Atomistic simulations of the TIP3P, SPC/E, TIP4P-Ew, and TIP4P/2005 water models are chosen as references for the REM process. Each AL water molecule is mapped onto its oxygen atom to represent the one-bead CG mX^{REM} water molecule, and each simulation system consists of a periodic cubic cell containing 1000 water molecules. All molecular dynamics (MD) simulations, including the simulations of the CG model in iteration of the REM process, are performed in LAMMPS. The equations of motion are

integrated using the velocity Verlet algorithm with time step of 1 and 10 fs for AL and CG simulations, respectively. The time step of 10 fs conserves the energy in microcanonical simulations with the mW model.[11] Both AL and CG simulations are evolved in the *NVT* ensemble using the Nosè−Hoover thermostat with T set to 298 K, with the volume for AL simulations derived from the ensemble average of the volume over 1 ns in equilibrated NpT ensemble at p = 1 atm and T = 298 K. The AL liquids are initially equilibrated for 1 ns under *NVT* conditions with T = 298 K controlled with the Nosè−Hoover thermostat, before collecting data from a further 50 ns of canonical AL simulations. The average box lengths derived from the equilibrated AL systems are then used in the *NVT* runs for CG simulations. The canonical simulations with the coarse-grained model for each iteration (i.e., parameter set) are evolved for 50 ns at 298 K. Configurations are sampled every 1 ps intervals for both AL and CG simulations. The damping constant of the thermostat and barostat are 1 and 5 ps, respectively, in the AL simulations and 8 and 40 ps, respectively, in the CG simulations. Periodic boundary conditions are used for all systems. About 100−200 REM iterations were needed for convergence of the CG parameter sets. The number of iterations depends on the selection of the initial parameter space. The properties of the AL models are validated with literature data.[1,45,47−50]

E. Calculation of Properties. We select a large number of thermodynamic, structural, and dynamic properties of the AL systems to build the property spaces. The structural properties considered here are radial distribution function (RDF), number of neighbors in the first coordination shell (neighbors), angular distribution function with the closest eight neighbors (ADF_8) and within the first shell ($ADF_{3.2Å}$, encompassing only the neighbors within 3.2 Å), and distribution of tetrahedral order parameter ($P(q_t)$).[51] The dynamics of the model is represented by the self-diffusion coefficient of the liquid at 298 K (D_{298K}).

The thermodynamic properties include (i) properties of the liquid phase, namely, density ($\rho_{298K;1atm}$) and enthalpy of vaporization (ΔH_{vap}) at 298 K (we consider enthalpy of vaporization to be a liquid property because the gas is assumed to be ideal), temperature of maximum density (TMD), and maximum density (ρ_{max}), and (ii) interfacial and two-phase properties, namely, surface tension at 298 K (σ_{298K}), melting temperature of hexagonal ice (T_m), enthalpy of fusion (ΔH_{melt}), entropy of fusion (ΔS_{melt}), density of liquid and ice I_h ($\rho_{liq@T_m}$ and $\rho_{I_h@T_m}$) at T_m, change in molar volume of melting (ΔV_{melt}), and the slope of the melting curve (dp/dT). We also evaluate the ratio and the difference between TMD and T_m (TMD/T_m and $TMD - T_m$), which are indicative of the location of the model in terms of the anomalous behavior of water.

The radial distribution function $g(R)$ between CG sites or between their corresponding O atom sites in the AL model was computed as

$$g(R) = \frac{V}{N^2}\left\langle \sum_i \sum_{j\neq i} \delta(R - R_{ij}) \right\rangle \tag{8}$$

where V is the volume, N is the number of water molecules, and R_{ij} is the distance between sites i and j. To quantify the accuracy of the CG models in reproducing the RDF of their reference AL models, we compute the residuals of the $g_{CG}(R)$ with respect to the $g_{AL}(R)$ as the integrated square of the difference between the two RDFs:

$$\text{res}_{RDF} = \sum_{i=1}^{N} |g_{CG}(R_i) - g_{AL}(R_i)|^2 \Delta R \tag{9}$$

where $N = R_c/\Delta R$, R_c is the cutoff distance, and ΔR is the distance between points sampled from the RDF. In this work, we use a cutoff R_c = 10 Å and sampled using ΔR = 0.01 Å. For comparison, we use the same equation to compute the residual of the RDF for the mW model ($g_{mW}(R)$) and for the AL models ($g_X(R)$) with respect to the experimental RDF ($g_{exp}(R)$) determined by Skinner et al.[52] The number of neighbors in the first coordination shell is calculated as the number of water neighbors within 3.5 Å.

The angular distribution functions are computed as

$$P(\theta) = \frac{1}{Nn_\theta}\left\langle \sum_{i=1}^{N} \sum_{j=1}^{n_c} \sum_{k\neq i}^{n_c-1} \delta(\theta - \theta_{ijk}) \right\rangle \tag{10}$$

where θ_{ijk} is the angle with i being the vertex, n_θ is the number of angles, n_c is the number of neighbors within the cutoff, and N is the number of particles. The difference between ADF_8 and $ADF_{3.2Å}$ is the number of neighbors accounted for in the calculations: ADF_8 accounts for angles with the eight closest neighbors, while $ADF_{3.2Å}$ accounts for angles with neighbors within a radius of 3.2 Å, i.e., the approximate position of the first minima in the RDF for the AL models. The residual of the ADF in the CG and AL models is calculated as the integrated square of the difference between the two ADFs

$$\text{res}_{ADF} = \sum_{i=1}^{180} |P_{CG}(\theta_i) - P_{AL}(\theta_i)|^2 \Delta\theta \tag{11}$$

where $\Delta\theta$ is the difference between points sampled from the ADF. In this work, we sample the ADF at 1° intervals over the range of 1−180°. For comparison, the residual of the ADF_8 for the mW model (ADF_{8mW}) and for the AL models (ADF_{8X}) with respect to the ADF (ADF_{8exp}) by Strässle et al.[53] derived from experimental data, is calculated as well using the same equation by replacing the ADF_{CG} and ADF_{AL} with RDF_{8mW} and ADF_{8exp}, respectively.

The tetrahedral order parameter associated with a water site i, q_t, is defined as[51]

$$q_t = 1 - \frac{3}{8}\sum_{j=1}^{3}\sum_{k=j+1}^{4}\left(\cos\theta_{ijk} + \frac{1}{3}\right)^2 \tag{12}$$

Here, θ_{ijk} is the angle between the side vectors R_{ij} and R_{ik}, where i is the vertex atom and j and k label the pairs among the four nearest water sites. Perfect tetrahedral coordination corresponds to q_t = 1.[51] The residual between the distribution of the tetrahedral order parameters derived from the CG simulation ($P_{CG}(q_t)$) and from the AL determinations ($P_{AL}(q_t)$) is calculated as the integrated square of the difference between the curves of the two $P(q_t)$

$$\text{res}_{P(q_t)} = \sum_{i=0}^{1} |P_{CG}(q_{t_i}) - P_{AL}(q_{t_i})|^2 \Delta q_t \tag{13}$$

where Δq_t = 0.01 is the difference between points sampled from the $P(q_t)$.

The density ρ is calculated as

$$\rho = NM/(N_A\langle V\rangle) \tag{14}$$

dx.doi.org/10.1021/ct500487h | J. Chem. Theory Comput. 2014, 10, 4104−4120

where N is the number of water molecules and M is the molecular mass of water, 18.015 g/mol.

The temperature of maximum density is calculated by performing isobaric cooling simulations at a rate of 1 K ns^{-1} from 230 to 70 K. The rate of change of the temperature is slow compared with the equilibration time of the liquid down to the temperatures below the TMD, so the liquid is in local equilibrium across the simulation.[11] Densities as a function of temperature, $\rho(T)$, are computed as a rolling average over 1 ns length intervals of the cooling simulation. The maximum density ρ_{max} is the density at TMD.

The enthalpy of vaporization of the monatomic liquids is calculated as

$$\Delta H_{vap} = H_{gas} - \langle E_{liq} + pV_{liq}\rangle \quad (15)$$

where R is the gas constant, H_{gas} is the total molar enthalpy of the gas, p is the pressure, E_{liq} is the total molar internal energy of the liquid, and V_{liq} is the molar volume of the liquid. Assuming the gases are ideal, the total molar enthalpy of the monatomic gas is $2.5RT$, where R is the gas constant and T is the temperature.

The melting temperature, T_m, of hexagonal ice (ice I_h) is determined through the method of direct phase coexistence in the NpT ensemble.[54] The simulations consist of 9216 atoms, with slabs of ice and liquid, each initially encompassing half of the molecules in the simulation cell, in contact with each other. The time step for the melting temperature simulations is 5 fs. The uncertainty in T_m is given by the gap between the higher temperature at which ice grows and the lowest temperature at which it melts, and is ±1 K in this study.

The enthalpy of fusion, ΔH_{melt}, is calculated as

$$\Delta H_{melt} = H_{liq} - H_{ice} \quad (16)$$

where H_{liq} and H_{ice} denote the molar enthalpy in the liquid water and the ice I_h, respectively, at the melting temperature of the model.

The entropy of fusion is calculated from the enthalpy of fusion divided by the melting temperature

$$\Delta S_{melt} = \frac{\Delta H_{melt}}{T_m} \quad (17)$$

The molar volume of melting, ΔV_{melt}, is calculated as

$$\Delta V_{melt} = V_{liq} - V_{ice} \quad (18)$$

where V_{liq} and V_{ice} denote the molar volume of the liquid water and ice at T_m.

The slope of the melting curve, dp/dT, is given by

$$\frac{dp}{dT} = \frac{\Delta S_{melt}}{\Delta V_{melt}} \quad (19)$$

The liquid–vapor surface tension, σ, is determined from the components of the pressure tensors tangential (p_t) and normal (p_n) to the liquid–vacuum interface averaged over 48 ns long simulations in the NVT ensemble of a liquid slab containing 1024 molecules,[55] i.e.,

$$\sigma = \frac{L_z}{2}[\langle p_n\rangle - \langle p_t\rangle] \quad (20)$$

where L_z is the length of the simulation cell in the direction perpendicular to the interface.

The self-diffusion coefficient of liquid water is computed from the root-mean-square displacement using Einstein–Kubo's relation

$$D = \lim_{\Delta t\to\infty} \frac{1}{6\Delta t}\langle |r(t+\Delta t) - r(t)|^2\rangle \quad (21)$$

where the ensemble average is over 8 ns long equilibrium simulations.

To quantify the overall agreement between the water models and the references, we implement Vega and Abascal's test of water models.[1] The score M quantifies the agreement between a water model and a reference (either an AL model or the experiment) in a scale from 10 (perfect agreement) to 0 according to[1]

$$M = \min\left\{\text{int}\left[10 - \text{abs}\left(\frac{(Y - Y_{ref})\times 100}{Y_{ref}\,\text{tol}}\right)\right], 0\right\} \quad (22)$$

where Y is the prediction of a given water model for a certain property, Y_{ref} is the corresponding value for the reference (the AL model or experiment), tol is the tolerance expressed as a percentage of the reference value Y_{ref}, and "int" is the nearest integer function. For res_{RDF}, res_{ADF_8}, $res_{ADF_{3.2Å}}$, $res_{P(q)}$, and TMD $- T_m$ that are already differences, tol is expressed as an absolute error value and the factor 100 appearing in eq 22 is dropped.[1] We use the same tolerances as in ref 1 when available. For the properties that are not presented in ref 1, the tolerances are selected as follows: for neighbors, res_{RDF}, and res_{ADF8} that are reproduced well with respect to the AL models, the tols are selected as the lowest values that result in 10 points for mTIP4P/2005^{REM} model; for $res_{ADF_{3.2Å}}$ that is reproduced moderately well, the tol is selected as the lowest value that results in 9 points for mTIP4P/2005^{REM} model; for $res_{P(q)}$ that is underestimated, the tol is selected as the lowest value that results in 4 points for the mTIP4P/2005^{REM} model; for ΔS_{melt} that is derived from $\Delta S_{melt} = \Delta H_{melt}/T_m$ (eq 17), the tol should be at least that of the ΔH_{melt} and T_m, so we chose the largest of the two, 5%. For ΔV_{melt} tol is selected as that of dp/dT[1], also 5%. Table 5 lists the full set of tol values.

III. RESULTS AND DISCUSSION

Atomistic level models usually display large variability in their accuracy in reproducing the experimental properties of a given system.[1] Thus, for each property, there is a set of values derived from different AL models (the value may be a function, e.g., the radial distribution function $g(r)$). We call the set of values for a given property the "AL property space", a one-dimensional set of values defining the coordinates in that space. Consider, for example, the set of AL water models TIP3P, SPC/E, TI4P-Ew, and TIP4P/2005; the four models produce quite similar values for the density of liquid at ambient conditions, ranging from 0.980 to 0.994 g/cm^3,[1,42−45] displaying a narrow AL density property space. For the melting temperature of ice I, on the other hand, the four AL water models give predictions ranging from 146 to 274 K,[1,45,47−49] resulting in a wide AL property space. The property space of CG models derived from a set of AL models, the "CG property space", is not necessarily the same as the one of the AL models used in their parametrization. If the AL and CG property spaces are represented by points in two parallel horizontal lines (we call this the "property mapping diagram"), ideally, the mapping lines from the AL to the CG property spaces should be vertical, which means that the

dx.doi.org/10.1021/ct500487h | J. Chem. Theory Comput. 2014, 10, 4104−4120

Table 1. Parameters of the CG Water Force Fields[a]

CG model	ε	σ	a_2	a_3	γ	B	λ	cos θ_0	cut$_2$ (Å)	cut$_3$ (Å)
mW[b]	6.189	2.3925	1.8	1.8	1.2	0.60222456	23.15	−0.333333	4.31	4.31
mTIP4P/2005^{REM}	53.4272	5.11162	0.809811	0.728778	0.319489	0.0537	1.19025	−0.377504	4.14	3.73
mTIP4P-Ew^{REM}	67.7509	5.86435	0.719956	0.642853	0.312486	0.0301567	1.04681	−0.403584	4.22	3.77
mTIP3P^{REM}	230.457	10.1602	0.45284	0.38487	0.251904	0.00306	0.358353	−0.554228	4.60	3.91
mSPC/E^{REM}	83.5737	6.4144	0.663822	0.586097	0.291321	0.0207826	0.762	−0.487217	4.26	3.76
mSPC/E$^{MS\text{-}CG}$[c]	1.0	1.0		3.7	1.2		13.1	−0.44	6.00	3.70

[a] cut$_2$ = $a_2\sigma$ and cut$_3$ = $a_3\sigma$ are the cutoffs of the two-body and three-body contributions to the potentials. p = 4 and A = 7.049556277 for all of the mX^{REM} models. [b] From ref 11. [c] From ref 13.

properties of the AL models are accurately reproduced by the CG models. Any deviations of the properties in CG models from those in AL ones will be reflected in the inclination of the mapping lines. Therefore, the mapping from each AL property space to the corresponding CG one gives explicit information on the ability of the coarse-graining approach to capture the properties of the reference models.

To facilitate the description of the mapping between the AL and CG property spaces, we define three characteristics of the property spaces: accuracy, order, and range. In this context, accuracy refers to the difference in a property between an AL model X and its CG counterpart, mX^{REM}. Order denotes the ordering of the models in terms of the values of the properties predicted by the set of models. For example, the melting temperatures of ice I$_h$ in the four AL water models, TIP3P, SPC/E, TIP4P-Ew, and TIP4P/2005, are 146, 215, 245.5, and 252.1 K,[1,45,47−49] respectively, which means that the order is TIP3P < SPC/E < TIP4P-Ew < TI4P/2005. Range denotes the width of the distribution of property values. For example, the range of the melting temperature in the AL property space is 106.5 K = 252.5 − 146 K.

The Results and Discussion section is organized following five major points. First, we investigate which properties of the AL models are well reproduced by the CG models derived by the REM method and which ones are not. Second, we disentangle which specific limitations arise from the coarse-graining methodology, from the monatomic nature of the CG models, and from the SW interaction potential form. Third, we assess whether the order of the AL property space is retained in the CG property space. Fourth, we investigate to which extent the range in each AL property space is reflected in the CG property space to assess whether it is conserved, contracted, or expanded. Finally, we score the overall ability of the different models to reproduce the properties of their reference atomistic models and experiment and assess the representability of the coarse-grained water models.

A. Parametrization and Properties of the mX^{REM} Coarse-Grained Water Models. We first generate the mX^{REM} CG water models for X = TIP4P/2005, TIP4P-Ew, TIP3P, and SPC/E. The initial potential parameters for the iterative optimization process were selected from the mW model. Table 1 lists the parameters for each mX^{REM} model, along with those for the monatomic CG water model with two-body and anisotropic three-body potentials derived from SPC/E water using MS-CG method, mSPC/E$^{MS\text{-}CG}$,[13,14] and for mW water.[11] The parameter spaces vary significantly from one model to another, but the potential curves (Figure 1), especially the two-body terms of mSPC/E^{REM}, mTIP4P-Ew^{REM}, and mTIP4P/2005^{REM}, are very similar, indicating that the SW parameters partly compensate with each other. We note that, different from the mW potential, the angle θ_o favored by the three-body term of the mX^{REM} and mSPC/E$^{MS\text{-}CG}$ is not the tetrahedral angle 109.48° but ranges from 112.2° to 123.7°, increasing in the order mTIP4P/2005^{REM} < mTIP4P-Ew^{REM} < mSPC/E$^{MS\text{-}CG}$ < mSPC/E^{REM} < mTIP3P^{REM}.

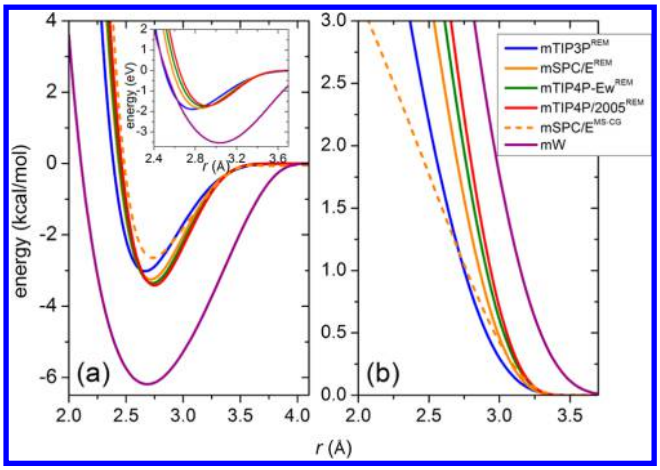

Figure 1. Radial dependence of the interaction potentials of the coarse-grained models: (a) two-body interaction term; (b) radial dependence of the three-body term (without the angular component) evaluated for $r_{ij} = r_{ik}$. The inset of panel (a) shows the sum of the potentials in panels (a) and (b).

We build the property spaces of the CG and AL models for a wide range of structural, dynamic, and thermodynamic properties (see Methods). Table 2 presents the reference experimental data, the results for the mW model, the results for the mX^{REM} models, and calculated properties for the AL models taken from our simulations and/or from the literature.[1,11,45,47−50,56,57] The properties of the mSPC/E$^{MS\text{-}CG}$ model derived from MS-CG method[13] are also presented for comparison. While each mX^{REM} model was parametrized from *NVT* simulations at the density at which the pressure of the corresponding X AL liquid is close to 1 atm, Table 2 shows that the pressure p^* of the mX^{REM} simulations at the same volume and temperature departs significantly from 1 atm. The values of ρ_{max}, TMD, ΔH_{vap}, T_m, TMD/T_m, ΔH_{melt}, ΔS_{melt}, ΔV_{melt}, dp/dT, and D_{298K} calculated at the pressure p^* are denoted with an asterisk, "*", in Table 2. The mappings from each AL to the corresponding CG property spaces are shown in Figure 2.

B. Accuracy of the Coarse-Grained Water Models. *B1. Structural Properties.* The REM method finds the CG potential parameters that minimize differences in sampling configurations in canonical simulations with the AL and CG models. As a result, it may be expected that the mX^{REM} models reproduce the structural properties of the reference model within the limitations of the form of the CG potential. The target radial distribution functions (Figure 3) are reproduced

dx.doi.org/10.1021/ct500487h | J. Chem. Theory Comput. 2014, 10, 4104−4120

Table 2. Properties of Water in Experiment and from Calculations with the AL and CG Models[a]

			TIP4P/2005		TIP4P-Ew		SPC/E			TIP3P	
property	exp	mW	AL	CG	AL	CG	AL	CG	MS-CG	AL	CG
neighbors	5.08	5.23	5.15	5.17*	5.12	5.14*	5.15	5.17*	5.26*	5.17	5.18*
res_{RDF} ($\times 10^{-3}$)	N/A	62[m]	(98[m])	7*	(115[m])	7*	(123[m])	7*	23*	(287[m])	6*
res_{ADF_8} ($\times 10^{-6}$)	N/A	89[m]	(109[m])	5*	(116[m])	5*	(115[m])	3*	13*	(131[m])	1*
$res_{ADF_{3.2Å}}$ ($\times 10^{-6}$)	N/A	N/A	N/A	41.51	N/A	38.70	N/A	41.88	112.75	N/A	19.38
$res_{P(q_t)}$ ($\times 10^{-3}$)	N/A	N/A	N/A	36.2*	N/A	34.4*	N/A	29.7*	67.1*	N/A	23.5*
D_{298K} (Å^2/ps)	0.2299	0.61	0.21	0.96*	0.25	1.01*	0.25	1.28*	1.57*	0.4	1.63*
p^* (atm)	1	1	−3	2929	12	2573	−4	2494	528	12	2000
V^*(Å^3/H_2O)	30.01	29.99	30.19	30.19	30.21	30.21	30.34	30.34	29.84	30.24	30.24
$\rho_{298K;1atm}$ (g cm^{-3})	0.997	0.998	0.998[d]	0.756	0.995[c]	0.758	0.994[e]	0.699	0.962	0.982[b]	0.643
ρ_{max} (g cm^{-3})	0.99997[k]	1.003[i]	1.0010[d]	1.02*	1.000[h]	1.03*	1.012[h]	1.04*	NF*[n]	1.038[h]	1.08*
TMD (K)	277.1	250[i]	278[d,e]	201*	273[h]	195*	241[h]	180*	NF*[n]	182[h]	151*
ΔH_{vap} (kcal mol^{-1})	10.52	10.67	11.98	4.76	11.66	466	11.69	4.32	4.70	10.49	3.86
ΔH_{vap}* (kcal mol^{-1})	10.52	10.67	11.98	3.80*	11.66	3.85*	11.69	3.58*	3.87*	10.49	3.41*
σ_{298K} (mN m^{-1})	71.99[l]	65.56	68.8[j]	6.56	63.3[j]	6.85	62.7[j]	4.89	20.70	51.6[j]	2.49
T_m (K)	273.15	274[i]	252.1[d,e]	208	245.5[f,g]	199	215.0[f−h]	177	114	145.6[g]	147
T_m* (K)	273.15	274[i]	252.1[d,e]	200*	245.5[f,g]	193*	215.0[f−h]	172*	104*	145.6[g]	143*
TMD/T_m	0.986	0.912	1.103	1.005*	1.112	1.010*	1.121	1.047*	NF*[n]	1.250	1.056*
TMD − T_m	3.95	−24	25.9	1*	27.5	2*	26	8*	NF*[n]	36.5	8*
ΔH_{melt} (kcal mol^{-1})	1.44	1.26[i]	1.16[d,e]	0.91*	1.05[f]	0.86*	0.74[d,e]	0.77*	0.38*	0.3[d,e]	0.58*
ΔS_{melt} (cal mol^{-1} K^{-1})	5.27	4.59	4.6	4.55*	4.28	4.46*	3.44	4.45*	3.75*	2.06	4.05*
ρ_{liq} (g cm^{-3}) (at T_m)	0.999	1.001[i]	0.993[d]	1.024*	0.992[f]	1.029*	1.011[f]	1.040*	1.141*	1.017[g]	1.079*
ρ_{I_h} (g cm^{-3}) (at T_m)	0.917	0.978[i]	0.921[d]	0.950*	0.936[g]	0.964*	0.950[g]	0.973*	0.973*	0.947[g]	1.021*
ΔV_{melt} (cm^3 mol^{-1})	−1.61[g]	−0.42[i]	−1.42[d]	−1.37*	−1.09[f,g]	−1.17*	−1.14[f,g]	−1.19*	−2.74*	−1.31[g]	−0.96*
$(dp/dT)_{melt}$ (atm K^{-1})	−135[d,e]	−448	−133[d,e]	−137*	−162[f,g]	−158*	−124[d−g]	−154 *	−57*	−65[d,e,g]	−175*

[a]Label CG indicates mXREM model. [b]Reference 42. [c]Reference 44. [d]Reference 45. [e]Reference 1. [f]Reference 47. [g]Reference 48. [h]Reference 49. [i]Reference 11. [j]Reference 50. [k]Reference 57. [l]Reference 58. [m]Compared to experimental distributions. [n]"NF*" means the density anomaly is not found at p^*. "p^*" denotes the calculated pressure for the X^{REM} models when performing an *NVT* simulation with the density set identical to that in the AL reference trajectory. The $g(r)$, $P(\theta)$, and $P(q)$ for the CG models are calculated in the *NVT* ensemble at the volumes of V^* listed in this table. The asterisk (*) means the CG property is calculated in the *NVT* ensemble at the corresponding V^* or in the *NpT* ensemble at the corresponding p^*. The values without the * are either the properties at 1 atm or the properties not related to the pressure. Note that the ΔH_{vap} for TIP4P/2005, TIP4P-Ew, and SPC/E are directly derived from the simulations, which do not include the self-polarization correction to the enthalpy of vaporization (the depolarization energy that needs to be invested when a water molecule is transferred from the bulk to the gas phase).[43,44,59] N/A indicates that the value of the property is not defined.

well by the mX^{REM} models (see residuals in Table 2) simulated at the same temperature and density as in their reference AL models. These reference volumes V^* correspond to very high pressures p^* for the mX^{REM} systems. The first peaks of the RDFs are reproduced very accurately, resulting in an almost identical number of neighbors in the first coordination shell (Table 2). A disagreement appears between the first well and the second peak, where there is a small ripple for all of the mX^{REM} models as well as the $mSPC/E^{MS\text{-}CG}$ model, which does not exist in the corresponding AL models. For two-body monatomic models of water it has been previously demonstrated[40] that rather small variations in the RDFs are associated with significant changes in the intermolecular potential. This is not the case for the mX^{REM} models, which interact through a sum of two-body and three-body potentials. While the RDFs for the mX^{REM} models are significantly different from each other (see inset of Figure 3a), all of the models have very similar two-body potentials (Figure 1a). This underscores the significant role of three-body interactions on reproducing the structure of liquid water.

The mX^{REM} models accurately reproduce the angular distribution functions involving the eight closest neighbors, ADF_8 (Figure 4, four upper panels) of the AL models at the same temperature and density. The most stringent ADFs accounting for the neighbors in the first coordination shell ($ADFs_{3.2Å}$) show a slight shift on the CG distribution near 103° relative to those of the AL models (Figure 4). The slight shift in $ADFs_{3.2Å}$ implies that water modeled with the CG mX^{REM} models has different tetrahedral order than their X AL counterparts. To explicitly quantify the agreement in tetrahedral order, we calculate the distribution of the tetrahedral order parameter $P(q_t)$ of the AL and CG models (Figure 5). As expected from $ADFs_{3.2Å}$, the tetrahedral order of the CG models is underestimated relative to the corresponding AL models. The distributions of the CG mX^{REM} are broader than for the reference AL water models and with a higher fraction of low-tetrahedrality molecules. The more the peaks in the $ADF_{3.2Å}$ shift, the less tetrahedral the local structure is (see the comparison of the $ADF_{3.2Å}$ and $P(q_t)$ of $mSPC/E^{REM}$ and $mSPC/E^{MS\text{-}CG}$ with SPC/E in Table 2 and Figures 4f and 5). In summary, the structural properties are overall well-reproduced by the mX^{REM} models at 298 K and the volume V^* of their AL parents (but not at 1 bar, where their density is 25−30% lower). There is a clear degradation in the agreement between the CG and their reference AL models when advancing in the comparison from the RDF, to the $ADF_{3.2Å}$, to the most stringent measure of tetrahedral order around the molecules, $P(q_t)$.

The underestimation of tetrahedral order in the mX^{REM} models (Figure 5) most likely originates from the short cutoff

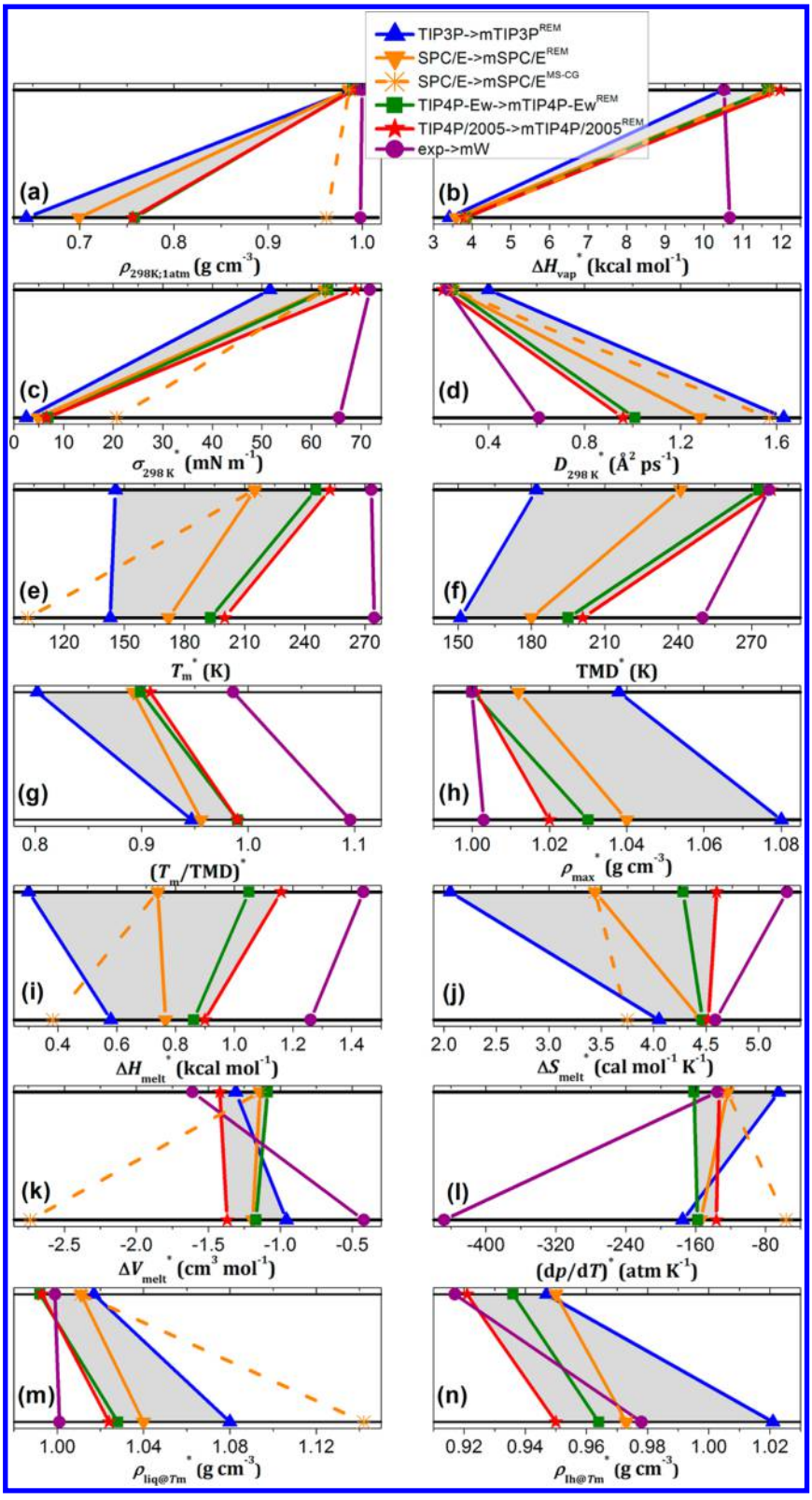

Figure 2. Property mapping diagrams for thermodynamic and dynamic properties. For each graph, the upper horizontal line indicates the atomistic level (AL) or experimental property space, and the lower horizontal line the coarse-grained property space. An asterisk after the name indicates that for the mX^{REM} and $mSPC/E^{MS\text{-}CG}$ models the property was evaluated at the pressure p^* that reproduces the density of the corresponding atomistic model at 1 atm. The areas in gray highlight the change of the range between AL and CG property spaces. Note that the difference between ΔH_{vap} of TIP3P and ΔH_{vap} of the other three AL models originates from the fact that TIP3P was parametrized based on different target ΔH_{vap} from the values used in parametrizing TIP4P/2005, TIP4P-Ew, and SPC/E.

σa_3 of the three-body interactions compared to those in the mW water model (Table 1). A recent analysis of the properties of SW monatomic water models as a function of parameter space revealed that potential cutoffs below 4.3 Å result in a

dx.doi.org/10.1021/ct500487h | J. Chem. Theory Comput. 2014, 10, 4104−4120

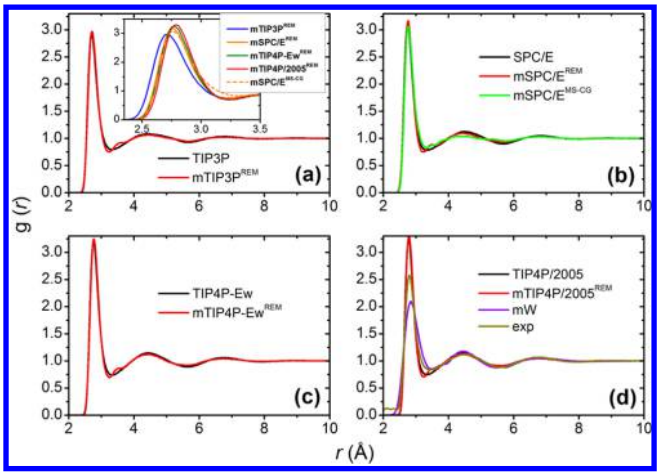

Figure 3. Radial distribution functions for the mX^{REM} and X models, where X = TIP3P, SPC/E, TIP4P-Ew, and TIP4P/2005. The RDFs for the $SPC/E^{MS\text{-}CG}$ and mW models as well as the experimental RDF[52] are also shown for comparison. The inset of panel (a) highlights the differences between the first peaks of different CG models.

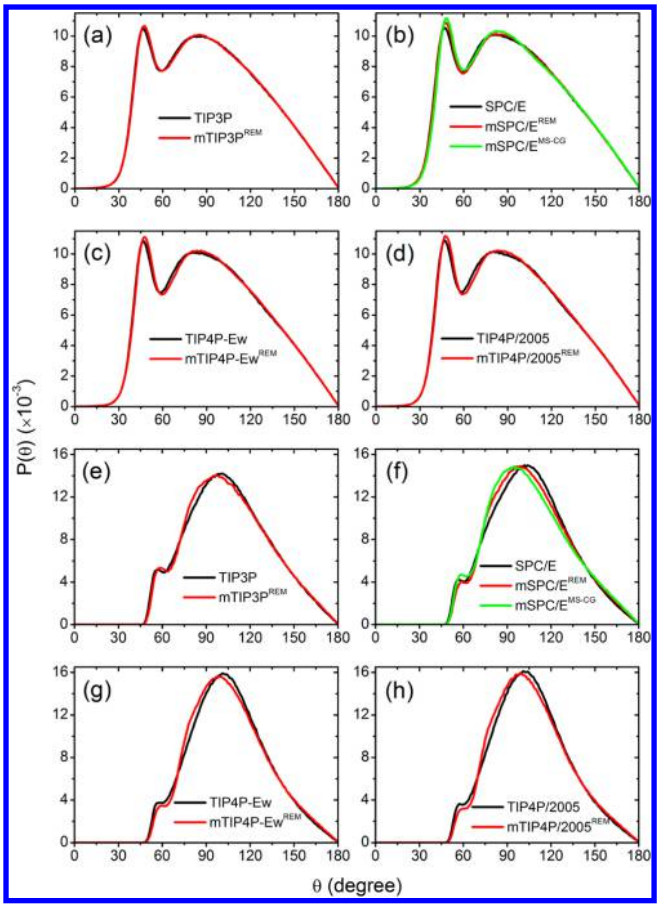

Figure 4. Comparison of angular distribution functions between X and mX^{REM} models: (a–d) ADFs with eight neighbors (ADF_8); (e–h) ADFs within the shell with $r \leq 3.2$ Å ($ADF_{3.2Å}$).

rapid degradation of the agreement of the properties of the monatomic model compared with experimental data.[18] The RDF of the AL models presents a narrower, sharper peak compared to the most recent experimental result. By reproducing the RDF of the AL models, the REM method

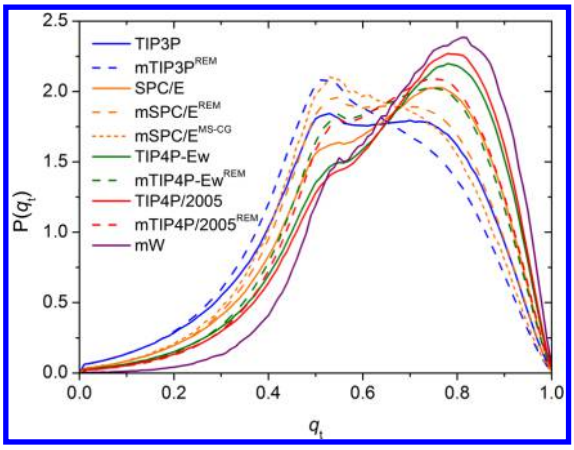

Figure 5. Comparison of the tetrahedral order parameter distributions for the models considered. q_t can vary between 0 (as in an ideal gas) and 1 (in a perfect tetrahedral network).[51]

pushes the parameters of the SW model into a region for which—as discussed in the next section—it performs poorly at reproducing the enthalpy and pressure of water in the condensed phases.[18]

B2. Thermodynamic Properties. The thermodynamic properties of the AL models are not reproduced as well as the structural properties by the mX^{REM} CG models, and there is also a significant variation in accuracy along these properties and along models (Table 2 and Figure 2). The pressures p^* of the CG models evolved in the *NVT* ensemble at the volume V^* which results in a pressure close to 1 atm in the corresponding AL reference trajectory, are highly overestimated in the mX^{REM} models. p^* of these models range from 2000 to about 3000 atm (Table 2). Recall that the CG mX^{REM} and $mSPC/E^{MS\text{-}CG}$ force fields are derived from canonical formalisms that are, in principle, insufficient to build a potential function for the calculation of the pressure in isothermal–isobaric simulations. mX^{REM} CG models evolved at 1 atm result in a severe underestimation (up to 35%) of the density of the liquid $\rho_{298K;1atm}$ (Table 2, Figure 2). To avoid comparing the AL properties with those of the CG models with highly reduced density at p = 1 atm, we evaluate a variety of properties of the CG models at p^* or V^* (depending on whether they are computed in the *NpT* or *NVT* simulation ensembles). For comparison, ΔH_{vap} and T_m at 1 atm are also presented in Table 2.

The enthalpy of vaporization of the mX^{REM} and $mSPC/E^{MS\text{-}CG}$ liquids is severely underestimated, by a factor of about 3 (Table 2 and Figure 2). Figure 1 shows that the mX^{REM} and $mSPC/E^{MS\text{-}CG}$ models have less attractive interaction potential than the mW model that produces good predictions for the enthalpy of vaporization of liquid water. Although the less positive three-body repulsion (Figure 1b) partially compensates for the higher energy of the two-body potential, the resulting total interaction energy in mX^{REM} and $mSPC/E^{MS\text{-}CG}$ models is still higher than in the mW potential (see inset of Figure 1a). This results in correspondingly higher potential energy predictions in the mX^{REM} models, which consequently leads to underestimation of the enthalpy of vaporization (see eq 15). For comparison, Table 2 also shows the ΔH_{vap} of mX^{REM} and $mSPC/E^{MS\text{-}CG}$ liquids at 1 atm. The predictions at 1 atm are higher, better, than those at p^*, but still less than 50% of the AL values. It has been shown for AL models that a lower prediction of the enthalpy of vaporization yields a lower prediction for the

dx.doi.org/10.1021/ct500487h | J. Chem. Theory Comput. 2014, 10, 4104–4120

liquid−vapor surface tension.[1] This correlation seems to also apply to the mX^{REM} models. Since the enthalpy of vaporization and the density of liquid at 1 atm are low in the mX^{REM} models, these liquids have little cohesion resulting in very rough liquid−vacuum interfaces and liquid−vapor surface tensions that are about 10% of the AL values (Table 2, Figure 2). A noticeable amount of molecules in the vapor phase in liquid−vapor mX^{REM} simulations indicates that these models have a substantial vapor pressure at 298 K. The ratio in vapor pressure of the model and experiments are given by the difference in enthalpy and entropy of the liquid in the model and experiments.[60] Monatomic water models are not expected to reproduce the vapor pressure of water because they lack a rotational contribution to the entropy. mW water reproduces the experimental enthalpy but underestimates the excess entropy of the liquid, resulting in a vapor pressure that is 2 orders of magnitude lower than in experiments.[60,61] The enthalpy of the mX^{REM} models is ∼40% of the experimental value, and because of the low density of the liquids at 1 bar, the entropy could also be higher than in experiments. These two factors result in a high vapor pressure of the mX^{REM} water models.

The mX^{REM} models display high variability in reproducing the melting properties (T_m, ΔH_{melt}, ΔS_{melt}, ΔV_{melt}, and dp/dT) at p^*, as can be gleaned from the slopes of the mapping lines in Figure 2. Overall, ice−liquid equilibrium properties are better reproduced than the thermodynamic properties of the liquid phase, although only simulations of the liquid state were used in the parametrization of the mX^{REM} models. Although the monatomic water models do not have a rotational contribution to the entropy, $\Delta S_{melt}{}^*$ of the of the mX^{REM} models at p^* are similar to those for the TIP4P/2005, TIP4P-Ew, and mW models at 1 bar, because the rotational contribution to the entropy of fusion of ice in atomistic water is small.[62] The melting temperatures and enthalpies of fusion of the mX^{REM} models at p^* are within the same range of those in the AL models. The enthalpy of the crystal phase is—as the one of the liquid—severely underestimated, but the CG models capture the difference in stabilization between these two condensed phases of water. The melting temperatures at 1 atm (Table 2) are higher than at p^*, consistent with the negative sign of the slope of the melting curve, dp/dT. The increase in melting temperature is less than predicted by $\Delta T_m = (dp/dT)^*\Delta T_m$, indicating that the slope of the melting curve increases with pressure. The actual value of $(dp/dT)^*$ is surprisingly well reproduced by the mX^{REM} CG models. This stems from a good prediction of both $\Delta S_{melt}{}^*$ and $\Delta V_{melt}{}^*$ (eq 19). The good agreement in $V_{melt}{}^*$ is due to a cancellation of errors as the densities of liquid and ice I_h (ρ_{liq} and ρ_{I_h}) are overestimated by almost the same amount (around 3%; see Table 2 and Figure 2). Overall, we find that the ability of the mX^{REM} coarse-grained models to reproduce the liquid−ice properties is better than for liquid−vapor ones. In the next section we show that the mX^{REM} models reproduce the anomalous behavior of water.

B3. Density Anomaly. Liquid water presents a wealth of anomalous behaviors in its thermodynamic, dynamic, and structural properties.[51,63,64] Some of these anomalies are shared with other tetrahedral liquids.[56,65−67] Among water thermodynamic anomalies, the best known is the existence of a TMD at which the density of the liquid reaches a maximum value (ρ_{max}) along an isobar. It has been shown that, for a liquid model, the existence of a density anomaly is associated with the presence of other thermodynamic, structural, and mobility anomalies.[56] Therefore, it is of importance to study whether the mX^{REM} models produce a density anomaly to assess their ability to replicate this characteristic behavior of water.

Figure 6 shows a sketch of the lines of density maxima of the liquid and melting of ice in the $T-p$ plane.[68,69] The sketch

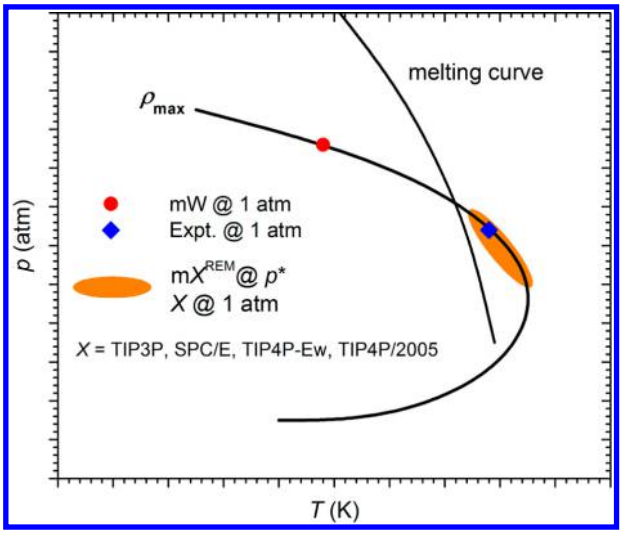

Figure 6. Schematic diagram for the locus of the density maximum ρ_{max} and melting curve in the $T-p$ plane following ref 69. The specific T and p for the maximum of TMD for AL and mW can be found in ref 56 and are reported in the main text. The TMD of the X AL models at 1 bar and and of the mX^{REM} CG models at p^* falls within the region (shaded in orange) for which the TMD is above the T_m. The data used to determine the range for the mX^{REM} models are presented in Table 3.

illustrates that the density anomaly exists only within a limited pressure domain, that the TMD increases with pressure until it reaches a maximum value, TMD^{max} (the nose of the curve of density maxima), and that at even higher pressures the line of maximum density of the liquid crosses, and then plunges below, the melting line. At 1 atm, the TMD of the AL models of this study is above T_m, which is also the case for real water. The experimental TMD and T_m of water cross at ∼500 atm.[68] The existence and locus of a TMD^{max} for real water at negative pressures has not yet been established.[70] TMD^{max} of the AL models occurs in the negative pressure region: TMD^{max} and its corresponding ρ_{max} are 257 K, 0.98 g cm^{-3} for TIP4P/2005 and 253 K, 1.00 g cm^{-3} for SPC/E.[56,64] The TMD^{max} of mW also occurs in the negative pressure region, at 271 K for a density of 0.95 g cm^{-3} ($p \sim -2000$ atm).[56]

None of the mX^{REM} models display a TMD at 1 atm, but they all display a density maximum at the pressure p^* that reproduces the density of the AL models at 1 atm. The $\rho_{max}{}^*$ of the mX^{REM} models are 1.8% to 4.05% larger and their TMD^* 17% to 28.6% lower than for the AL models evaluated at 1 atm. We did not find a density anomaly in mSPC/E^{MS-CG} at 1 atm, 528 atm (the corresponding p^*), or 2000 atm. It has been previously demonstrated that for monatomic water models that interact through a pair potential that reproduces well the radial distribution function of a reference atomistic model, the coarse-grained pair potential has to be density-dependent to capture the existence of a density anomaly.[10] While a CG potential should be state-dependent to produce an accurate representation of the multidimensional PMF of the reference model, the

dx.doi.org/10.1021/ct500487h | J. Chem. Theory Comput. 2014, 10, 4104−4120

Table 3. Pressure Dependence of the Temperatures of Maximum Density of the Coarse-Grained Models

mW		mTIP4P/2005^{REM}		mTIP4P-Ew^{REM}		mSPC/E^{REM}		mTIP3P^{REM}	
p (atm)	TMD (K)	p (atm)	TMD (K)	p (atm)	TMD (K)	p (atm)	TMD (K)	p (atm)	TMD (K)
−1000	256	1	none	1	none	1	none	1	none
−500	253	1000	198	1000	195	2000	179	1500	153
1[a]	250	2000	206	2000	203	2250	181	2000[a]	151
500	244	2929[a]	201	2573[a]	195	2494[a]	180	2500	148

[a]Corresponds to p^* of the model presented in Table 2.

mX^{REM} and mW water models parametrized at a single state point reproduce well the pair distribution function of their reference models and the existence of a density anomaly for a variety of pressures (see subsequent discussion). These results stress the important role of three-body interactions on improving the transferability and representability of CG water models.

We use the ratio TMD/T_m and the pressure dependence of TMD (Table 3) to locate the AL and CG models in the sketch of Figure 6. Note that the locations for mW and the AL model and experiment are determined at 1 atm, while the locations for mX^{REM} models are determined at p^*. The TMD* of the mX^{REM} models is above their corresponding T_m^*, which locate them above the crossover region in Figure 6, same as the AL models and the experiments at 1 bar, and in contrast with the results for mW water, for which TMD is 24 K below T_m at 1 bar.[11] Interestingly, the ratio TMD*/T_m^* and the difference (TMD* − T_m) from the mX^{REM} models are closer to experiment than their AL parent models.

B4. Dynamical Properties. The self-diffusion coefficients at 298 K (D_{298K}) are highly overestimated for all of the mX^{REM} and mSPC/E$^{MS\text{-}CG}$, almost three to four times the corresponding AL values (Table 2). There are three factors that contribute to the high diffusivity of the coarse-grained models. The first one is intrinsic to the monatomic nature of the coarse-grained models and originates from the lack of hydrogen atoms that slow down the reorientation of the atomistic water molecules.[11] The coarse-grained molecules move in a smoother, less repulsive, free energy surface than the fully atomistic water molecules. The second is related to the low cohesive energy of the mX^{REM} and mSPC/E$^{MS\text{-}CG}$ models. It has been shown that a lower prediction of enthalpy of vaporization yields a higher prediction of self-diffusion coefficient.[1] The very low enthalpy of vaporization in mX^{REM} and mSPC/E$^{MS\text{-}CG}$ increases the self-diffusion coefficient of the mX^{REM} and mSPC/E$^{MS\text{-}CG}$ liquids, as can be appreciated by comparison with the D_{298K} of mW water, which reproduces ΔH_{vap}. The third, subtler, factor is related to the low tetrahedral order in the mX^{REM} and mSPC/E$^{MS\text{-}CG}$ liquids, as the mobility of water is correlated to the existence of topological defects in the tetrahedral network of the liquid.[71]

C. Comparison of the Order in the Property Spaces of the CG and AL Models. The REM approach is capable of distinguishing and capturing even the tiny differences between the reference AL models in structural, dynamic and thermodynamic properties. For the RDFs (Figure 3) and ADFs (Figure 4), there is no doubt that the order is retained because the residuals between RDFs of the X^{REM} CG and X AL models are smaller than the residuals among AL models. For the distribution of the tetrahedral order parameters, which are not reproduced as accurately as the RDFs and the ADFs, their order is conserved as well. Figure 5 shows that the tetrahedral order parameters in the CG models decrease in the order mTIP4P/2005^{REM} > mTIP4P-Ew^{REM} > mSPC/E^{REM} > mTIP3P^{REM}, which is the same as for the AL models. The tetrahedral order of the mX^{REM} models mirrors the order of the radial contribution to the three-body potentials (Figure 1). It also reflects the deviation of the favored angle θ_o (eq 3) from the perfectly tetrahedral angle 109.48° (Table 1).

For the thermodynamic and dynamic properties, the order is reflected in the property mapping diagrams. There is no crossing between the mapping lines for all of the diagrams of X → mX^{REM} except ΔV_{melt}^* and the related slope of the melting curve $(dp/dT)^*$. Although the enthalpy of vaporization, the self-diffusion coefficient, and the surface tension are reproduced so poorly, their orders in the AL parameter spaces are retained accurately. Another interesting observation is that the mapping lines for most thermodynamic properties (Figure 2) as well as the tetrahedral order (Figure 5) have the same order: TIP3P < SPC/E < TIP4P-Ew < TIP4P/2005 (or the reverse one: TIP4P/2005 < TIP4P-Ew < SPC/E < TIP3P) from lower to higher values in the property mapping diagrams. The constrained order demonstrates that there is a strong correspondence between the structural, dynamic, and thermodynamic properties of the water models and that this correspondence is not significantly affected by their poor representability. On the other hand, the strong correspondence indicates that improving the prediction of one property by adjusting the form of the force field can strongly affect the predictions for other properties. This gives some insight on why the top-down approaches can yield models with so different overall predictions for a variety of properties just by adjusting the predictions of a handful of emergent phenomena.

D. Comparison of the Range of the CG and AL Property Spaces. We now assess whether the range for each property is contracted, conserved, or expanded upon coarse-graining. For the structural properties, the ranges are overall conserved since these properties are quite accurately reproduced. Instead, for the thermodynamic properties these ranges vary significantly (see Figure 2). As mentioned above, the CG mX^{REM} potentials were constructed from canonical ensemble atomistic simulation data and do not reproduce the pressure of the AL models at the density of the parameterization. Therefore, it is not surprising that the range in the $\rho_{298K;1atm}$ property space expands due to the widening of the range in the property space of pressure (Table 2). However, for the other CG property spaces, only the ranges in D_{298K}^*, ρ_{max}^*, $\rho_{liq@T_m}^*$ and $\rho_{I_h@T_m}^*$ CG property spaces expand, while all of the others contract toward specific regions (Figure 2). ΔH_{melt}^*, for example, contracts toward ∼0.8 kcal/mol and ΔS_{melt}^* contract toward 4.5 cal mol^{-1} K^{-1}, which indicates that coarse-graining reduces the range of these properties. The contraction in the space of these properties could be due to a limitation of the resolution of the CG representation and the CG potential form, because CG models have less interaction sites, fewer degrees of freedom, and a simpler potential forms to describe the more

dx.doi.org/10.1021/ct500487h | J. Chem. Theory Comput. 2014, 10, 4104−4120

detailed structures and interaction potentials of the reference AL models. We note, however, that there is a significant variability in the evolution of the range of properties and, as Figure 2 shows, contraction of the property range is not universal upon coarse-graining.

E. Score of the CG Models. Vega and Abascal scored five popular water AL models according to a wide range of properties that include most of those considered in this study plus a wide array of liquid−vapor properties, phase behavior at high pressure, and properties that are specific to atomistic models (e.g., dielectric constant, rotational times). From higher to lower, the scores they computed for the AL models are 7.2 for TIP4P/2005, 5.1 for SPC/E, 4.7 for TIP4P, 3.7 for TIP5P, and 2.7 for TIP3P.[1] A score of 10 would indicate that the AL model reproduces accurately the experimental results. We implement the scoring scheme proposed by Vega and Abascal's (see Methods) to establish how well the AL and 5 CG models discussed in this work model the behavior of water. We first compare the score of all models with respect to experiment and then the score of the mX^{REM} CG models with respect to their AL references.

Table 4 presents the average score over all properties of the present study for the AL and CG with respect to experiment.

Table 4. Average Score of the CG and AL Models with Respect to Experiment

model	score[a]
TIP4P/2005	7.8
TIP4P-Ew	6.9
mW	6.1
SPC/E	5.6
mTIP4P/2005^{REM}	4.2
mTIP4P-Ew ^{REM}	3.6
TIP3P	3.2
mSPC/E ^{REM}	3.2
mTIP3P^{REM}	2.1

[a]Averaged over the set of experimentally available properties listed in Table 5. Note that several properties of the mX^{REM} models were evaluated at p^*, as shown in Table 5.

The scores for TIP4P/2005, SPC/E, and TIP3P in Table 4 are about half a point higher than for the wider set of properties considered in ref 1. TIP4P-Ew scores between TIP4P/2005 and SPC/E model; a significant improvement over the performance of TIP4P, which ranks below SPC/E.[1] The agreement between mX^{REM} models and experiment degrades, unsurprisingly, with the score of the X AL model. It is noteworthy that—for the set of properties considered here—the best CG models outperform the least accurate but extensively used AL models. The accuracy of mW in reproducing experimental properties of water ranks between TIP4P-Ew and SPC/E, while mTIP4P/2005^{REM} and mTIP4P-Ew^{REM} score between SPC/E and TIP3P. These results demonstrate that, for certain applications, coarse-grained models can offer an alternative to atomistic level simulations that is not only computationally much more efficient (by at least 2 orders of magnitude for the SW monatomic water models) but also competitive in accuracy.

Table 5 scores the accuracy of the mX^{REM} CG water models in reproducing the properties of their parent AL models, along with the scores for mW, mTIP4P/2005^{REM}, and TIP4P/2005 with respect to experiment. The faithfulness of the mX^{REM} models to their AL parents (4.5−4.7 for mTIP4P/2005^{REM}, mTIP4P-Ew^{REM}, and mSPC/E^{REM} and 3.2 for mTIP3P^{REM}) is considerably lower than the faithfulness of mW to experiment (score 6.1). In the remainder of this work, we analyze in more detail the performance and limitations of the coarse-grained models.

All mX^{REM} CG models score very high marks on structural properties, except for the most demanding measure of tetrahedral order, $P(q_t)$. The average scores for structural properties are 8.6 for mTIP4P/2005^{REM}, 8.8 for mTIP4P-Ew^{REM}, 8.6 for mSPC/E^{REM}, and 9.0 for mTIP3P^{REM}. mW scores an average of 8 for the structural properties (which do not include $P(q_t)$, because it is not available from experiments). The high scores in structural properties, along with extensive studies of mW water, indicate that the sum of two- and three-body terms in the functional form of the SW potential is able to mimic the hydrogen-bonded structures of water in the liquid, ice, amorphous ice, and clathrate phases.[11,62,72−88] CG water models based on isotropic pair potentials do not stabilize the tetrahedrally coordinated water crystals. The introduction of a three-body function more flexible than in the SW potential, e.g., the basis sets of ref 15, should improve the ability of the mX^{REM} CG models to reproduce the angular and tetrahedral distributions of the AL references.

All CG models score 0 on reproducing the dynamics of their references; this low score cannot be lifted by reparametrization or change in the functional form of the potential, because it has a physical origin: it reflects the loss of the frictional force that the hydrogen atoms (i.e., the rotation of water) exerts on the translational mobility. Coarse-grained models move in a smoother free energy surface than atomistic models, leading to an intrinsic limit in the ability of CG models to reproduce the dynamics of their references. The ability of a CG model to reproduce the relative time scales between different processes is a better measure of their usefulness in modeling physical processes. Studies of diffusivity vs crystallization times,[62,88] and diffusion coefficients or resident times of different molecules in the same system,[77,80,89] for the mW water model indicate that these ratios can be well-represented in a coarse-grained SW water model. More work is needed to determine to which extent these results hold for the mX^{REM} models.

The mX^{REM} and mW coarse-grained water models display quite different abilities to represent the thermodynamic properties of their references, although they use the same mapping and functional form of the SW potential. The average scores of the thermodynamic properties are 6.1 for mW, 3.9 for mTIP4P/2005^{REM}, 3.9 for mTIP4P-Ew^{REM}, 3.7 for mSPC/E^{REM}, and 1.8 for mTIP3P^{REM}. There is only a narrow region in parameter space for which the SW model reproduces simultaneously the experimental density and enthalpy of vaporization of liquid water.[18] That region in parameter set is such that the monatomic model closely reproduces the experimental oxygen−oxygen RDF of liquid water. However, the first peak of the RDF of the AL models of this study is sharper and narrower than the one in the experimental RDF, pushing the parameters of the SW CG models into a region where they are unable to reproduce the enthalpy of the AL models. Interestingly, the properties of TIP4P/2005 are better reproduced by mW (score 5.4) than by mTIP4P/2005^{REM} (score 4.7, Table 5). We conclude that a small compromise in the accuracy of structural properties offers the possibility of increasing the overall accuracy and representability of the coarse-grained water models.

Table 5. Scores by Property[a]

			X^{REM} compared to their AL references				AL and CG compared to experiment		
	tol (%)	property[b]	$mTIP4P/2005^{REM}$	$mTIP4P\text{-}Ew^{REM}$	$mSPC/E^{REM}$	$mTIP3P^{REM}$	TIP4P/2005	$mTIP4P/2005^{REM}$	mW
structural	2.5	neighbors	**10**	**10**	**10**	**10**	**9**	**9**	**9**
	30×10^{-3}[c]	res_{RDF}	**10**	**10**	**10**	**10**	7	6	**8**
	30×10^{-6}[c]	res_{ADF_8}	**10**	**10**	**10**	**10**	6	7	7
	30×10^{-6}[c]	$res_{ADF_{3.2Å}}$	**9**	**9**	**9**	**9**	-	-	-
	6×10^{-3}[c]	$res_{P(q)}$	4	5	4	**6**	-	-	-
dynamic	0.5	ln $D_{298\ K}$	0	0	0	0	**8**	0	0
thermodynamic	0.5	$\rho_{298\ K;1\ atm}$	0	0	0	0	9	0	**10**
	0.5	ρ_{max}	2	**4**	**4**	2	**10**	6	9
	2.5	TMD	0	0	0	**3**	**10**	0	6
	2.5	ΔH_{vap}	0	0	0	0	4	0	**9**
	2.5	$\sigma_{298\ K}$	0	0	0	0	**8**	0	6
	2.5	T_m	2	1	2	**9**	7	0	**10**
	5 K[c]	TMD − T_m	5	5	**6**	4	6	**9**	4
	5	ΔH_{melt}	6	6	**9**	0	6	3	**8**
	5	ΔS_{melt}	**10**	9	4	0	7	7	7
	0.5	ρ_{liq} (at T_m)	**4**	3	**4**	0	9	5	**10**
	0.5	ρ_{Ih} (at T_m)	4	4	**5**	0	**9**	3	0
	5	ΔV_{melt}	**9**	9	**9**	5	**8**	7	0
	5	$(dp/dT)_{melt}$	9	**10**	5	0	**10**	**10**	0
final score			4.7	4.7	4.5	3.2	7.8	4.2	6.1

[a]Best score for each property with respect to the AL or experimental reference is shown with bold font. [b]The CG properties (except $\rho_{298K;1atm}$ and σ_{298K}) are calculated at p^* and are presented in Table 2. [c]tol for this property is absolute, not a percentage.

The limitations observed for the CG models developed with the REM are shared by the model coarse-grained from mSPC/$E^{MS\text{-}CG}$ with the three-body term of the SW potential along with a flexible spline two-body function. To test the influence of the form of the two-body potential we also parametrize the $mTIP4P4/2005^{REM}$ model with $p = 9$ in the two-body term. The resulted CG models show negligible differences on the two-body potential curves and, concomitantly, also on the properties of the models parametrized with the parameter $p = 4$. The interaction length (cutoff) of the potential also has a high impact on the representability of the CG models: as the interaction length decreases, the enthalpy and density suffer and adjusting parameters to fix one diminishes the accuracy in the other, although the structure can still be well-reproduced.[18] Although the cutoffs (Table 1) and the potential curves (Figure 1) of the two-body terms in the mX^{REM} and mSPC/$E^{MS\text{-}CG}$ models approximately retain the value of ∼4.3 Å shown in ref 18 to be optimum for reproducing experimental water properties with the SW form, the cutoffs for the three-body potentials of the mX^{REM} and mSPC/$E^{MS\text{-}CG}$ range from 3.70 to 3.91 Å (Table 1), far below the value for which the SW potential can reproduce water properties.[18] Decreasing the cutoff of cosine−quadratic three-body potential leads to a minimization of the relative entropy, suggesting that the SW form of the three-body potential is not appropriate to reproduce the orientational order of the water molecules in the AL models. The role of the functional form and cutoff of the three-body potential on the representability of the mX^{REM} CG models of water will be the subject of future work.

IV. CONCLUSION

The present work investigates the features of the relative entropy minimization method in capturing the structural, thermodynamic, and dynamic properties of reference atomistic water models (X = TIP3P, SPC/E, TIP4P-Ew, and TIP4P/2005) into coarse-grained monatomic water models mX^{REM} that interact through the Stillinger−Weber potential. The diffusion coefficients of the monatomic coarse-grained models are—as expected—significantly larger than in the atomistic models, and tuned by both the cohesive energy and degree of tetrahedral order in the liquid. The mX^{REM} water models reproduce the structural properties of the atomistic level models quite well, while the thermodynamic properties are mostly under- or overestimated. The inability of the models to simultaneously reproduce the structural and thermodynamic properties might be improved by using a more flexible three-body potential form or by changing the ensemble in which the models are parametrized. The present work shows that the ranges of most of the thermodynamic property spaces contract when the model is coarse-grained based on the REM approach, but this is not a universal result for all properties. Most significantly, our analysis demonstrates that, although the mX^{REM} models do not accurately reproduce several thermodynamic properties of the AL water models, the REM method is able to capture well the difference in equilibrium properties between liquid and ice (although the latter was not included in the parametrization) as well as the existence of even tiny differences in properties among the AL water models. We conjecture this is due to a strong correspondence between the structural and the thermodynamic properties, which is not significantly affected by the low representability of the coarse-grained models.

The REM method captures the structural properties as well as the small differences of properties between similar atomistic models. Nevertheless, it does not reproduce the enthalpy and density of the water models at 1 bar. The inability of the models to reproduce the density of water at ambient conditions originates from the fact that the REM optimization is performed in the canonical ensemble. One option to correctly reproduce the density at ambient conditions would be to parametrize the model in the isothermal−isobaric ensemble, which requires the extension of the formalism of the REM method to deal with the relationships between the volumes of the system and the potential parameters. Another option would be to correct the potential derived by canonical REM to reproduce the pressure. Systematic procedures for pressure correction using the pair distribution function $g(r)$ have been developed and successfully implemented for two-body potentials.[33,40] Triplet correlations are significant for the structure, thermodynamics, and anomalies of water.[90] The development of pressure corrections that account for the triplet contributions to the virial component of the pressure should be developed and tested for their ability to produce coarse-grained monatomic water models with improved representability.

We conjecture that the lower accuracy and representability of the mX^{REM} models compared to mW may arise from the insufficient flexibility in the cosine quadratic form of the three-body SW potential to represent the structure of the AL water models. It is worth investigating to which extent the quality of the coarse-grained models derived with the REM method can be improved by using a more flexible three-body potential form. Das and Andersen developed a variational approach to optimize flexible three-body potentials within the MS-CG method and applied it to develop a monatomic coarse-grained model based on SPC/E.[15] They found improvements in the description of water structural correlations with respect to those obtained using the cosine quadratic form of the Stillinger−Weber potential. We expect that this should lead to a more accurate description of the thermodynamics of the reference model. Unfortunately, ref 15 does not report thermodynamic properties nor the coefficients for the two- and three-body potentials; therefore we are unable to compare the results of that model with mSPC/E^{REM} and mSPC/E^{MS-CG}. In addition to the use of more flexible basis sets for the potentials, a combination of the REM method with a top-down approach may be helpful. For example, based on the force field derived from the REM method, one can tune the parameters by using an uncertainty quantification approach[18] to get a better prediction for some of the thermodynamic properties. Sacrificing the enthalpy of vaporization leads to a better overall score in atomistic rigid nonpolarizable water models.[1,43] The better overall agreement between mW and TIP4P/2005 than between mTIP4P/2005^{REM} and TIP4P/2005 indicates that the overall quality of the coarse-grained model can be improved by relaxing in the accuracy of certain properties, most notably the pair distribution function.

All classical force fields, including the AL models considered in this work, have significant representability issues that prevent them from faithfully reproducing the properties of more detailed water models or the experiment. There is, however, a clear order of accuracy of atomistic models represented by their scores in the test of water models of Vega and Abascal.[1] The overall accuracy of the AL and CG models evaluated in this work in reproducing experimental water properties is as follows, from better to worse: TIP4P/2005 > TIP4P-Ew > mW > SPC/E > mTIP4P/2005^{REM} > mTIP4P-Ew^{REM} > TIP3P > mSPC/E^{REM} > mTIP3P^{REM}. There are several noteworthy aspects of this ranking. First, the order of the mX^{REM} models follows the one of the corresponding X AL models. The degradation in the scores is correlated with the decrease in tetrahedrality of the model within the AL and CG sets. Second, the top-down mW model ranks above the bottom-up mX^{REM} models, posing the question of whether more accurate water models are derived—when feasible—from experimental data rather than from approximate high-quality atomistic models. It is worth investigating to which extent the quality of the coarse-grained models derived with the REM method can be improved by using more sophisticated water models as references, such as the recently developed CC-pol,[91] WHBB,[92] HBB2-pol,[93] and MB-pol.[94−96] It is also still an open question what is the maximum score that can be achieved by a monatomic water model with anisotropic interactions: a recent top-down reparametrization of mW using uncertainty quantification and considering the radial distribution function instead of the temperature of melting as target properties yielded a model, mW$_{UQ}$, with properties and accuracy very similar to the original mW.[18] Third, and most significant, the ranking demonstrates that some coarse-grained water models can score higher than widely used atomistic level water models. This indicates that coarse-grained monatomic water models with anisotropic interactions can be competitive in accuracy with AL models for the study of a wide range of properties and phenomena at less than 1/100th of the computational cost.[11]

It is important to recall that models of water are not water. The Hamiltonians used in classical simulations are not even related to the Hamiltonian that determines the behavior of real water. The systematic study of the properties and phase behavior of sets of water models offers invaluable insight into how water-like behavior arises from relatively simple effective interactions.[11,97−106] Several studies have focused on understanding water behavior in the broader context of tetrahedral liquids.[11,56,64−67,102,107,108] All of the coarse-grained models of this study mimic, to some extent, properties of water. The set of well-characterized coarse-grained water models of this work should be useful for the elucidation of factors that control the emergence of distinct water-like behavior, such as the hierarchy[51] of thermodynamic, dynamic, and structural anomalies, as well as the relationship between triplet correlations, anomalies, polyamorphism, and crystallization in water.

AUTHOR INFORMATION

Corresponding Authors

*(V.M.) E-mail: Valeria.Molinero@utah.edu.

*(R.B.) E-mail: r.baron@utah.edu.

Notes

The authors declare no competing financial interest.

ACKNOWLEDGMENTS

We gratefully acknowledge Luca Larini for kindly providing us with the interaction potentials of the SPC/E^{MS-CG} model, M. Scott Shell for his generous advice on the REM method, and Charusita Chakravarty for productive discussions. This work was supported by the National Science Foundation through Award CHE-1305427 and by The University of Utah through a Seed Grant Award. We thank the Center for High Performance

Computing at The University of Utah for technical support and allocation of computer time.

REFERENCES

(1) Vega, C.; Abascal, J. L. F. Simulating water with rigid non-polarizable models: A general perspective. *Phys. Chem. Chem. Phys.* **2011**, *13*, 19663−19688.

(2) Guillot, B. A reappraisal of what we have learnt during three decades of computer simulations on water. *J. Mol. Liq.* **2002**, *101*, 219−260.

(3) Bernal, J.; Fowler, R. A theory of water and ionic solution, with particular reference to hydrogen and hydroxyl ions. *J. Chem. Phys.* **1933**, *1*, 515−548.

(4) Darré, L.; Machado, M. R.; Pantano, S. Coarse-grained models of water. *Wiley Interdiscip. Rev.: Comput. Mol. Sci.* **2012**, *2*, 921−930.

(5) Hadley, K. R.; McCabe, C. Coarse-grained molecular models of water: a review. *Mol. Simul.* **2013**, *38*, 671−681.

(6) Molinero, V.; Goddard, W. M3B: A coarse grain force field for molecular simulations of malto-oligosaccharides and their water mixtures. *J. Phys. Chem. B* **2004**, *108*, 1414−1427.

(7) Johnson, M. E.; Head-Gordon, T.; Louis, A. A. Representability problems for coarse-grained water potentials. *J. Chem. Phys.* **2007**, *126*, No. 144509.

(8) Johnson, M. E.; Head-Gordon, T. Assessing thermodynamic-dynamic relationships for waterlike liquids. *J. Chem. Phys.* **2009**, *130*, No. 214510.

(9) Izvekov, S.; Voth, G. A. Multiscale coarse graining of liquid-state systems. *J. Chem. Phys.* **2005**, *123*, No. 134105.

(10) Chaimovich, A.; Shell, M. S. Anomalous waterlike behavior in spherically-symmetric water models optimized with the relative entropy. *Phys. Chem. Chem. Phys.* **2009**, *11*, 1901−1915.

(11) Molinero, V.; Moore, E. B. Water Modeled As an Intermediate Element between Carbon and Silicon. *J. Phys. Chem. B* **2009**, *113*, 4008−4016.

(12) Dias, C. L.; Ala-Nissila, T.; Grant, M.; Karttunen, M. Three-dimensional "Mercedes-Benz" model for water. *J. Chem. Phys.* **2009**, *131*, No. 054505.

(13) Larini, L.; Lu, L.; Voth, G. A. The multiscale coarse-graining method. VI. Implementation of three-body coarse-grained potentials. *J. Chem. Phys.* **2010**, *132*, No. 164107.

(14) Larini, L.; Shea, J.-E. Double Resolution Model for Studying TMAO/Water Effective Interactions. *J. Phys. Chem. B* **2013**, *117*, 13268−13277.

(15) Das, A.; Andersen, H. C. The multiscale coarse-graining method. IX. A general method for construction of three body coarse-grained force fields. *J. Chem. Phys.* **2012**, *136*, No. 194114.

(16) Zipoli, F.; Laino, T.; Stolz, S.; Martin, E.; Winkelmann, C.; Curioni, A. Improved coarse-grained model for molecular-dynamics simulations of water nucleation. *J. Chem. Phys.* **2013**, *139*, No. 094501.

(17) Noid, W. G. Perspective: Coarse-grained models for biomolecular systems. *J. Chem. Phys.* **2013**, *139*, No. 090901.

(18) Jacobson, L. C.; Kirby, R. M.; Molinero, V. How Short Is Too Short for the Interactions of a Water Potential? Exploring the Parameter Space of a Coarse-Grained Water Model using Uncertainty Quantification. *J. Phys. Chem. B* **2014**, *118*, 8190−8202.

(19) Maerzke, K. A.; Siepmann, J. I. Transferable Potentials for Phase Equilibria−Coarse-Grain Description for Linear Alkanes. *J. Phys. Chem. B* **2011**, *115*, 3452−3465.

(20) Rossi, G.; Monticelli, L.; Puisto, S. R.; Vattulainen, I.; Ala-Nissila, T. Coarse-graining polymers with the MARTINI force-field: Polystyrene as a benchmark case. *Soft Matter* **2011**, *7*, 698−708.

(21) Schmid, F. Toy amphiphiles on the computer: What can we learn from generic models? *Macromol. Rapid Commun.* **2009**, *30*, 741−751.

(22) Monticelli, L.; Kandasamy, S. K.; Periole, X.; Larson, R. G.; Tieleman, D. P.; Marrink, S.-J. The MARTINI Coarse-Grained Force Field: Extension to Proteins. *J. Chem. Theory Comput.* **2008**, *4*, 819−834.

(23) DeVane, R.; Shinoda, W.; Moore, P. B.; Klein, M. L. Transferable Coarse Grain Nonbonded Interaction Model for Amino Acids. *J. Chem. Theory Comput.* **2009**, *5*, 2115−2124.

(24) Zwanzig, R. Memory Effects in Irreversible Thermodynamics. *Phys. Rev.* **1961**, *124*, 983−992.

(25) Hijón, C.; Español, P.; Vanden-Eijnden, E.; Delgado-Buscalioni, R. Mori−Zwanzig formalism as a practical computational tool. *Faraday Discuss.* **2009**, *144*, 301.

(26) Kirkwood, J. G. Statistical Mechanics of Fluid Mixtures. *J. Chem. Phys.* **1935**, *3*, 300−313.

(27) Murtola, T.; Bunker, A.; Vattulainen, I.; Deserno, M.; Karttunen, M. Multiscale modeling of emergent materials: Biological and soft matter. *Phys. Chem. Chem. Phys.* **2009**, *11*, 1869−1892.

(28) Noid, W. G.; Chu, J. W.; Ayton, G. S.; Krishna, V.; Izvekov, S.; Voth, G. A.; Das, A.; Andersen, H. C. The multiscale coarse-graining method. I. A rigorous bridge between atomistic and coarse-grained models. *J. Chem. Phys.* **2008**, *128*, No. 244115.

(29) Rudzinski, J. F.; Noid, W. G. Coarse-graining entropy, forces, and structures. *J. Chem. Phys.* **2011**, *135*, No. 214101.

(30) Christ, C. D.; Mark, A. E.; van Gunsteren, W. F. Basic ingredients of free energy calculations: A review. *J. Comput. Chem.* **2009**, 1569−1582.

(31) Tschöp, W.; Kremer, K.; Batoulis, J.; Bürger, T.; Hahn, O. Simulation of polymer melts. I. Coarse-graining procedure for polycarbonates. *Acta Polym.* **1998**, *49*, 61−74.

(32) Ashbaugh, H. S.; Patel, H. A.; Kumar, S. K.; Garde, S. Mesoscale model of polymer melt structure: Self-consistent mapping of molecular correlations to coarse-grained potentials. *J. Chem. Phys.* **2005**, *122*, No. 104908.

(33) Reith, D.; Pütz, M.; Müller-Plathe, F. Deriving effective mesoscale potentials from atomistic simulations. *J. Comput. Chem.* **2003**, *24*, 1624−1636.

(34) Lyubartsev, A. P.; Laaksonen, A. Calculation of effective interaction potentials from radial distribution functions: A reverse Monte Carlo approach. *Phys. Rev. E* **1995**, *52*, 3730−3737.

(35) Lyubartsev, A. P.; Laaksonen, A. On the Reduction of Molecular Degrees of Freedom in Computer Simulations. *Lect. Notes Phys.* **2004**, *640*, 219−244.

(36) Shell, M. S. The relative entropy is fundamental to multiscale and inverse thermodynamic problems. *J. Chem. Phys.* **2008**, *129*, No. 144108.

(37) Chaimovich, A.; Shell, M. S. Coarse-graining errors and numerical optimization using a relative entropy framework. *J. Chem. Phys.* **2011**, *134*, No. 094112.

(38) Carmichael, S. P.; Shell, M. S. A New Multiscale Algorithm and Its Application to Coarse-Grained Peptide Models for Self-Assembly. *J. Phys. Chem. B* **2012**, *116*, 8383−8393.

(39) Izvekov, S.; Voth, G. A. A Multiscale Coarse-Graining Method for Biomolecular Systems. *J. Phys. Chem. B* **2005**, *109*, 2469−2473.

(40) Wang, H.; Junghans, C.; Kremer, K. Comparative atomistic and coarse-grained study of water: What do we lose by coarse-graining? *Eur. Phys. J. E: Soft Matter Biol. Phys.* **2009**, *28*, 221−229.

(41) Stillinger, F. H.; Weber, T. A. Computer-Simulation of Local Order in Condensed Phases of Silicon. *Phys. Rev. B* **1985**, *31*, 5262−5271.

(42) Jorgensen, W. L.; Chandrasekhar, J.; Madura, J. D.; Impey, R. W.; Klein, M. L. Comparison of simple potential functions for simulating liquid water. *J. Chem. Phys.* **1983**, *79*, 926−935.

(43) Berendsen, H. J. C.; Grigera, J. R.; Straatsma, T. P. The missing term in effective pair potentials. *J. Phys. Chem.* **1987**, *91*, 6269−6271.

(44) Horn, H. W.; Swope, W. C.; Pitera, J. W.; Madura, J. D.; Dick, T. J.; Hura, G. L.; Head-Gordon, T. Development of an improved four-site water model for biomolecular simulations: TIP4P-Ew. *J. Chem. Phys.* **2004**, *120*, 9665−9678.

(45) Abascal, J. L. F.; Vega, C. A general purpose model for the condensed phases of water: TIP4P/2005. *J. Chem. Phys.* **2005**, *123*, No. 234505.

(46) Plimpton, S. J. Fast Parallel Algorithms for Short-Range Molecular Dynamics. *J. Comput. Phys.* **1995**, *117*, 1−19.

(47) Abascal, J. L. F.; Sanz, E.; García Fernández, R.; Vega, C. A potential model for the study of ices and amorphous water: TIP4P/Ice. *J. Chem. Phys.* **2005**, *122*, No. 234511.
(48) Vega, C.; Sanz, E.; Abascal, J. L. F. The melting temperature of the most common models of water. *J. Chem. Phys.* **2005**, *122*, No. 114507.
(49) Vega, C.; Abascal, J. L. F. Relation between the melting temperature and the temperature of maximum density for the most common models of water. *J. Chem. Phys.* **2005**, *123*, No. 144504.
(50) Sakamaki, R.; Sum, A. K.; Narumi, T.; Yasuoka, K. Molecular dynamics simulations of vapor/liquid coexistence using the non-polarizable water models. *J. Chem. Phys.* **2011**, *134*, No. 124708.
(51) Errington, J. R.; Debenedetti, P. G. Relationship between structural order and the anomalies of liquid water. *Nature* **2001**, *409*, 318−321.
(52) Skinner, L. B.; Huang, C.; Schlesinger, D.; Pettersson, L. G. M.; Nilsson, A.; Benmore, C. J. Benchmark oxygen-oxygen pair-distribution function of ambient water from x-ray diffraction measurements with a wide Q-range. *J. Chem. Phys.* **2013**, *138*, No. 074506.
(53) Strässle, T.; Saitta, A. M.; Godec, Y. L.; Hamel, G.; Klotz, S.; Loveday, J. S.; Nelmes, R. J. Structure of Dense Liquid Water by Neutron Scattering to 6.5 GPa and 670 K. *Phys. Rev. Lett.* **2006**, *96*, No. 067801.
(54) Wang, J.; Yoo, S.; Bai, J.; Morris, J. R.; Zeng, X. C. Melting temperature of ice Ih calculated from coexisting solid-liquid phases. *J. Chem. Phys.* **2005**, *123*, No. 036101.
(55) Vega, C.; de Miguel, E. Surface tension of the most popular models of water by using the test-area simulation method. *J. Chem. Phys.* **2007**, *126*, No. 154707.
(56) Jabes, S. B.; Nayar, D.; Dhabal, D.; Molinero, V.; Chakravarty, C. Water and Other Tetrahedral Liquids: Order, Anomalies and Solvation. *J. Phys.: Condens. Matter* **2012**, *24*, No. 284116.
(57) *Handbook of Chemistry and Physics*, 81th ed.; CRC Press: Boca Raton, FL, USA, 2000.
(58) Pallas, N. R.; Harrison, Y. An automated drop shape apparatus and the surface tension of pure water. *Colloids Surf.* **1990**, *43*, 169−194.
(59) Abascal, J. L. F.; García Fernández, R.; MacDowell, L. G.; Sanz, E.; Vega, C. Ice: A fruitful source of information about liquid water. *J. Mol. Liq.* **2007**, *136*, 214−220.
(60) Factorovich, M. H.; Molinero, V.; Scherlis, D. A. A simple grand canonical approach to compute the vapor pressure of bulk and finite size systems. *J. Chem. Phys.* **2014**, *140*, No. 064111.
(61) Factorovich, M. H.; Molinero, V.; Scherlis, D. A. Vapor pressure of water nanodroplets. *J. Am. Chem. Soc.* **2014**, *136*, 4508−4514.
(62) Moore, E. B.; Molinero, V. Structural Transformation in Supercooled Water Controls the Crystallization Rate of Ice. *Nature* **2011**, *479*, 506−508.
(63) Debenedetti, P. G. Supercooled and glassy water. *J. Phys.: Condens. Matter* **2003**, *15*, R1669−R1726.
(64) Agarwal, M.; Alam, M. P.; Chakravarty, C. Thermodynamic, Diffusional, and Structural Anomalies in Rigid-Body Water Models. *J. Phys. Chem. B* **2011**, *115*, 6935−6945.
(65) Angell, C. A.; Bressel, R. D.; Hemmati, M.; Sare, E. J.; Tucker, J. C. Water and its anomalies in perspective: Tetrahedral liquids with and without liquid−liquid phase transitions. *Phys. Chem. Chem. Phys.* **2000**, *2*, 1559−1566.
(66) Hujo, W.; Jabes, B. S.; Rana, V. K.; Chakravarty, C.; Molinero, V. The Rise and Fall of Anomalies in Tetrahedral Liquids. *J. Stat. Phys.* **2011**, *145*, 293−312.
(67) Nayar, D.; Chakravarty, C. Water and water-like liquids: Relationships between structure, entropy and mobility. *Phys. Chem. Chem. Phys.* **2013**, *15*, 14162−14177.
(68) Angell, C. A.; Kanno, H. Density Maxima in High-Pressure Supercooled Water and Liquid Silicon Dioxide. *Science* **1976**, *193*, 1121−1122.
(69) Poole, P. H.; Saika-Voivod, I.; Sciortino, F. Density minimum and liquid−liquid phase transition. *J. Phys.: Condens. Matter* **2005**, *17*, L431−L437.
(70) Meadley, S. L.; Angell, C. A., Water and its relatives: The stable, supercooled and particularly the stretched, regimes. *[physics.chem-ph]* **2014**arXiv:1404.4031.
(71) Sciortino, F.; Geiger, A.; Stanley, H. E. Network defects and molecular mobility in liquid water. *J. Chem. Phys.* **1992**, *96*, 3857−3865.
(72) Johnston, J. C.; Kastelowitz, N.; Molinero, V. Liquid to quasicrystal transition in bilayer water. *J. Chem. Phys.* **2010**, *133*, No. 154516.
(73) Johnston, J. C.; Molinero, V. Crystallization, Melting, and Structure of Water Nanoparticles at Atmospherically Relevant Temperatures. *J. Am. Chem. Soc.* **2012**, *134*, 6650−6659.
(74) Moore, E. B.; Molinero, V. Is it Cubic? Ice Crystallization from Deeply Supercooled Water. *Phys. Chem. Chem. Phys.* **2011**, *13*, 20008−20016.
(75) Bullock, G.; Molinero, V. Low-Density Liquid Water is the Mother of Ice: on the Relation between Mesostructure, Thermodynamics and Ice Crystallization in Solutions. *Faraday Discuss.* **2013**, *167*, 371−388.
(76) Kastelowitz, N.; Johnston, J. C.; Molinero, V. The anomalously high melting temperature of bilayer ice. *J. Chem. Phys.* **2010**, *132*, No. 124511.
(77) Jacobson, L. C.; Molinero, V. A methane-−ater model for coarse-grained simulations of solutions and clathrate hydrates. *J. Phys. Chem. B* **2010**, *114*, 7302−7311.
(78) Jacobson, L. C.; Hujo, W.; Molinero, V. Amorphous Precursors in the Nucleation of Clathrate Hydrates. *J. Am. Chem. Soc.* **2010**, *132*, 11806−11811.
(79) Nguyen, A. H.; Jacobson, L. C.; Molinero, V. Structure of the clathrate/solution interface and mechanism of cross-nucleation of clathrate hydrates. *J. Phys. Chem. C* **2012**, *116*, 19828−19838.
(80) DeMille, R. C.; Molinero, V. Coarse-grained ions without charges: Reproducing the solvation structure of NaCl in water using short-ranged potentials. *J. Chem. Phys.* **2009**, *131*, No. 034107.
(81) Le, L.; Molinero, V. Nanophase Segregation in Supercooled Aqueous Solutions and Their Glasses Driven by the Polyamorphism of Water. *J. Phys. Chem. A* **2011**, *115*, 5900−5907.
(82) Moore, E. B.; Allen, J. T.; Molinero, V. Liquid-Ice Coexistence Below the Melting Temperature for Water Confined in Hydrophilic and Hydrophobic Nanopores. *J. Phys. Chem. C* **2012**, *116*, 7507−7514.
(83) Jacobson, L. C.; Hujo, W.; Molinero, V. Thermodynamic stability and growth of guest-free clathrate hydrates: A low-density crystal phase of water. *J. Phys. Chem. B* **2009**, *113*, 10298−10307.
(84) Nguyen, A. H.; Molinero, V. Stability and Metastability of Bromine Clathrate Polymorphs. *J. Phys. Chem. B* **2013**, *117*, 6330−6338.
(85) Limmer, D. T.; Chandler, D. Theory of Amorphous Ices. *Proc. Natl. Acad. Sci. U. S. A.* **2014**, DOI: 10.1073/pnas.1407277111.
(86) Moore, E. B.; de la Llave, E.; Welke, K.; Scherlis, D. A.; Molinero, V. Freezing, Melting and Structure of Ice in a Hydrophilic Nanopore. *Phys. Chem. Chem. Phys.* **2010**, *12*, 4124−4134.
(87) Moore, E. B.; Molinero, V. Growing Correlation Length in Supercooled Water. *J. Chem. Phys.* **2009**, *130*, 244505−244512.
(88) Moore, E. B.; Molinero, V. Ice Crystallization in Water's "No-Man's Land". *J. Chem. Phys.* **2010**, *132*, No. 244504.
(89) Demille, R. C.; Cheatham, T. E., III; Molinero, V. A coarse-grained model of DNA with explicit solvation by water and ions. *J. Phys. Chem. B* **2011**, *115*, 132−142.
(90) Singh, M.; Dhabal, D.; Nguyen, A. H.; Molinero, V.; Chakravarty, C. Triplet correlations dominate the transition from simple to tetrahedral liquids. *Phys. Rev. Lett.* **2014**, *112*, No. 147801.
(91) Bukowski, R.; Szalewicz, K.; Groenenboom, G. C.; van der Avoird, A. Predictions of the Properties of Water from First Principles. *Science* **2007**, *315*, 1249−1252.
(92) Wang, Y.; Huang, X.; Shepler, B. C.; Braams, B. J.; Bowman, J. M. Flexible, ab initio potential, and dipole moment surfaces for water.

I. Tests and applications for clusters up to the 22-mer. *J. Chem. Phys.* **2011**, *134*, No. 094509.
(93) Medders, G. R.; Babin, V.; Paesani, F. A Critical Assessment of Two-Body and Three-Body Interactions in Water. *J. Chem. Theory Comput.* **2013**, *9*, 1103−1114.
(94) Babin, V.; Medders, G. R.; Paesani, F. Development of a "First Principles" Water Potential with Flexible Monomers. II: Trimer Potential Energy Surface, Third Virial Coefficient, and Small Clusters. *J. Chem. Theory Comput.* **2014**, *10*, 1599−1607.
(95) Babin, V.; Leforestier, C.; Paesani, F. Development of a "First Principles" Water Potential with Flexible Monomers: Dimer Potential Energy Surface, VRT Spectrum, and Second Virial Coefficient. *J. Chem. Theory Comput.* **2013**, *9*, 5395−5403.
(96) Medders, G. R.; Babin, V.; Paesani, F. Development of a "First-Principles" Water Potential with Flexible Monomers. III. Liquid Phase Properties. *J. Chem. Theory Comput.* **2014**, to be submitted for publication.
(97) Ben-Naim, A. Statistical Mechanics of "Waterlike" Particles in Two Dimensions. I. Physical Model and Application of the Percus−Yevick Equation. *J. Chem. Phys.* **1971**, *54*, No. 3682.
(98) Jagla, E. A. Core-softened potentials and the anomalous properties of water. *J. Chem. Phys.* **1999**, *111*, 8980−8986.
(99) Buldyrev, S. V.; Kumar, P.; Debenedetti, P. G.; Rossky, P. J.; Stanley, H. E. Water-like solvation thermodynamics in a spherically symmetric solvent model with two characteristic lengths. *Proc. Natl. Acad. Sci. U. S. A.* **2007**, *104*, 20177−20182.
(100) Buldyrev, S. V.; Malescio, G.; Angell, C. A.; Giovambattista, N.; Prestipino, S.; Saija, F.; Stanley, H. E.; Xu, L. Unusual phase behavior of one-component systems with two-scale isotropic interactions. *J. Phys.: Condens. Matter* **2009**, *21*, No. 504106.
(101) Yan, Z.; Buldyrev, S.; Giovambattista, N.; Stanley, H. Structural Order for One-Scale and Two-Scale Potentials. *Phys. Rev. Lett.* **2005**, *95*, No. 130604.
(102) Prasad, S.; Chakravarty, C. Onset of simple liquid behaviour in modified water models. *J. Chem. Phys.* **2014**, *140*, No. 164501.
(103) Chatterjee, S.; Debenedetti, P. G.; Stillinger, F. H.; Lynden-Bell, R. M. A computational investigation of thermodynamics, structure, dynamics and solvation behavior in modified water models. *J. Chem. Phys.* **2008**, *128*, No. 124511.
(104) Lynden-Bell, R. M.; Head-Gordon, T. Solvation in modified water models: Towards understanding hydrophobic effects. *Mol. Phys.* **2006**, *104*, 3593−3605.
(105) Lynden-Bell, R. M.; Debenedetti, P. G. Computational investigation of order, structure, and dynamics in modified water models. *J. Phys. Chem. B* **2005**, *109*, 6527−6534.
(106) Dill, K. A.; Truskett, T. M.; Vlachy, V.; Hribar-Lee, B. Modeling water, the hydrophobic effect, and ion solvation. *Annu. Rev. Biophys. Biomol. Struct.* **2005**, *34*, 173−199.
(107) Molinero, V.; Sastry, S.; Angell, C. A. Tuning of Tetrahedrality in a Silicon Potential Yields a Series of Monatomic (Metal-like) Glass Formers of Very High Fragility. *Phys. Rev. Lett.* **2006**, *97*, No. 075701.
(108) Agarwal, M.; Singh, M.; Sharma, R.; Parvez Alam, M.; Chakravarty, C. Relationship between structure, entropy, and diffusivity in water and water-like liquids. *J. Phys. Chem. B* **2010**, *114*, 6995−7001.